THE DESIGN OF AN INSTRUMENT TO MEASURE VERTICALLY AVERAGED OCEANIC CURRENTS USING GEOMAGNETIC ELECTRIC FIELDS

by

PETER FRANK PORANSKI

B.S., Engineering Science
Newark College of Engineering
(1970)

SUBMITTED IN PARTIAL FULFILLMENT OF THE REQUIREMENTS FOR THE DEGREE OF OCEAN ENGINEER

at the

MASSACHUSETTS INSTITUTE OF TECHNOLOGY

and the

WOODS HOLE OCEANOGRAPHIC INSTITUTION

and

MASTER OF SCIENCE IN OCEAN ENGINEERING

at the

MASSACHUSETTS INSTITUTE OF TECHNOLOGY

August 1972

Signature of Author.....
Joint Program in Ocean Engineering, Massachusetts Institute of Technology - Woods Hole Oceanographic Institution, and Department of Ocean Engineering, Massachusetts Institute of Technology, August 1972

Certified by.....
Thesis Supervisor

Certified by.....
Thesis Supervisor

Accepted by.....
Chairman, Joint Committee for Ocean Engineering, Massachusetts Institute of Technology - Woods Hole Oceanographic Institution

THE DESIGN OF AN INSTRUMENT TO MEASURE VERTICALLY AVERAGED OCEANIC CURRENTS USING GEOMAGNETIC ELECTRIC FIELDS

by

Peter Frank Poranski

Submitted in partial fulfillment of the requirements for the degree of Ocean Engineer at the Massachusetts Institute of Technology and the Woods Hole Oceanographic Institution and Master of Science in Ocean Engineering at the Massachusetts Institute of Technology.

ABSTRACT

A bottom mounted electromagnetic current meter measures the vertically-averaged conductivity-weighted velocity. This measurement complements free-fall relative velocity profiles and is valuable for transport determination and dynamics studies. Such an instrument has been designed to measure the three components of the electric field, E_x, E_y, and E_z. Salt bridges used with switched electrodes permit the induced electromotive forces to be measured with only a short baseline; eight foot arms are planned. The first part of this report covers the theory behind the bottom mounted electric field meter. The second part discusses the design of the instrument as well as a brief description of the prototype bottom mounted electric field meter.

Thesis Supervisor: Dr. Albert J. Williams III
Title : Assistant Scientist

Thesis Supervisor: J. Harvey Evans
Title : Professor of Naval Architecture

ACKNOWLEDGEMENTS

The successful completion of the project described here was due in part to the combined efforts of many of the W.H.O.I. staff, and especially Dr. Thomas Sanford, Dr. Albert Williams III, and Mr. Robert Drever for their helpful advice and encouragement during the project; and to Mrs. Karen Pires for her patient typing of this manuscript.

TABLE OF CONTENTS

TABLE OF CONTENTS (Cont.)

LIST OF ILLUSTRATIONS

LIST OF ILLUSTRATIONS (cont.)

INTRODUCTION

The problem, simply stated, is to design an instrument to be placed on the bottom of the ocean that will measure the true horizontal and vertical current velocity vectors by electromagnetic techniques. To accomplish this it is desired to measure the three components of the electric field E_x, E_y, and E_z that are generated by oceanic currents. An additional measurement, also desired, is the local current velocity in the vicinity of the instrument. A bottom mounted electric field meter is important because of its ability to obtain mass transport information. There is, at present, no simple means of obtaining this data.

The design target was for the instrument to be deployed as its own mooring or interchangeably on a conventional buoy mooring. It was to remain on station, self sufficient, for at least one week in the early stages of development and ultimately, in excess of one month.

The first section of this report will cover the basic theory behind the bottom mounted electric field meter. Parts of this section have been taken from "Short Arm Electric Field Measurements of Ocean Currents," Williams et al (1972), of which the writer is one of the co-authors. The second section will discuss the designed instrument and contain a brief description of the prototype bottom mounted electric field meter.

A. THEORY BEHIND THE BOTTOM MOUNTED ELECTRIC FIELD METER

I. General Principles

Let us start with a simple example. In Figure 1 let ab be a movable conductor of length L. Assume a uniform magnetic field of induction $\vec{B}$ extending in the positive Z-direction. Now let the conductor be moved at a velocity $\vec{V}$ in the positive Y-direction. According to Ampere's Law, the free charge q in the wire will experience a force $\vec{F}$ in the plus X-direction such that

$$F = qVB \tag{1}$$

From the definition of electric intensity

$$E = \frac{\vec{F}}{q} \tag{2}$$

We can then obtain the motional electric field in the X-direction

$$\vec{E} = VB \tag{3}$$

Since this motional field exists only in the moving conductor ab of length L, we have for the emf around the circuit

$$\text{emf} = \oint \vec{E} \cdot d\vec{s} = VLB \tag{4}$$

The above simple case may now be generalized for the case where $\vec{V}$ is the velocity of any element $d\vec{s}$ of a circuit and $\vec{V}$, $d\vec{s}$, and $\vec{B}$ are not necessarily mutually perpendicular. In general then, we have that

$$\vec{E} = \vec{V} \times \vec{B} \tag{5}$$

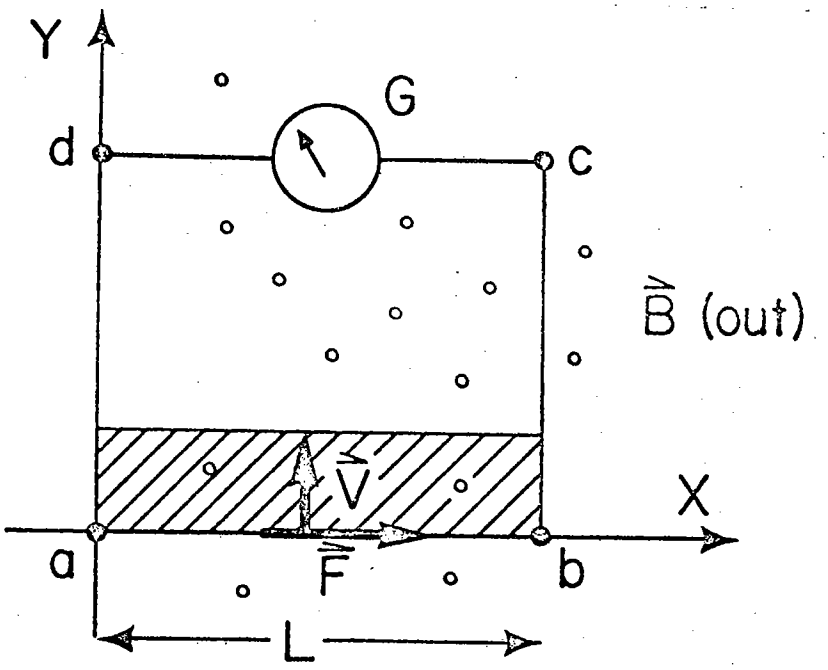

Figure 1. Motional emf

and the electromotive force (emf) is defined by

$$\text{emf} = \oint \vec{V} X \vec{B} \cdot d\vec{s} \tag{6}$$

In the case of the moving conductor, just described, the induced emf in the conductor would cause a current I to flow such that

$$\text{emf} = IR \tag{7}$$

where R is the resistance of the conductor. For a continuous medium

$$\vec{E} = \vec{J}/\sigma \tag{8}$$

where $\vec{J}$ is the current density within the medium and σ is the electrical conductivity of the material. The above relation is by no means universally valid, and the range of current densities over which it holds is called the linear range of the particular material.[1] In general then, for the case of continuous media it is assumed that there is an electric current density such that $\vec{J}/\sigma$ around any closed

circuit just equals the circulation of the induced emf. From equation 6 we then have that

$$\oint(\vec{V}X\vec{B} - \vec{J}/\sigma)\cdot d\vec{s} = 0 \tag{9}$$

and it then follows that

$$\phi(p) = \int_0^p (\vec{V}X\vec{B} - J/\sigma)\cdot d\vec{s} \tag{10}$$

where ϕ is an electrical potential defined at each point p in space and

$$\nabla\phi = \vec{V}X\vec{B} - \vec{J}/\sigma \tag{11}$$

where ∇ is the vector differential operator.

II. Physical Principles

Sea water is an electrolyte of high conductivity because of the abundance of highly dissociated salts. The motion of this electrolyte through the earth's magnetic field produces electromagnetic effects similar to a moving solid conductor. In general, an electrolyte moving with a velocity $\vec{V}$ will interact with a magnetic field at rest, with an intensity $\vec{B}$, to produce an electric field of intensity $\vec{E}$, fully determined by the vector cross product

$$\vec{E} = \vec{V}X\vec{B} \tag{12}$$

From this equation one can see that a knowledge of the velocity and the magnetic field uniquely determine the electric field. In the oceanographic sense the velocity is the unknown that is desired,

therefore, if one can measure the electric field, and obtain the magnetic field from published data, the velocity can be obtained.

Assume now a uniform stream of sea water moving at a constant velocity $\vec{V}$ in an infinitely long trough of rectangular cross section and width L (see Figure 2). The magnetic field is assumed to be perpendicular to the flow in the positive $\hat{z}$-direction. The walls of the channel in this example are assumed to replace the external path in Figure 1. Assume also that there are two potentiometers, one stationary and one moving with the fluid. In the following

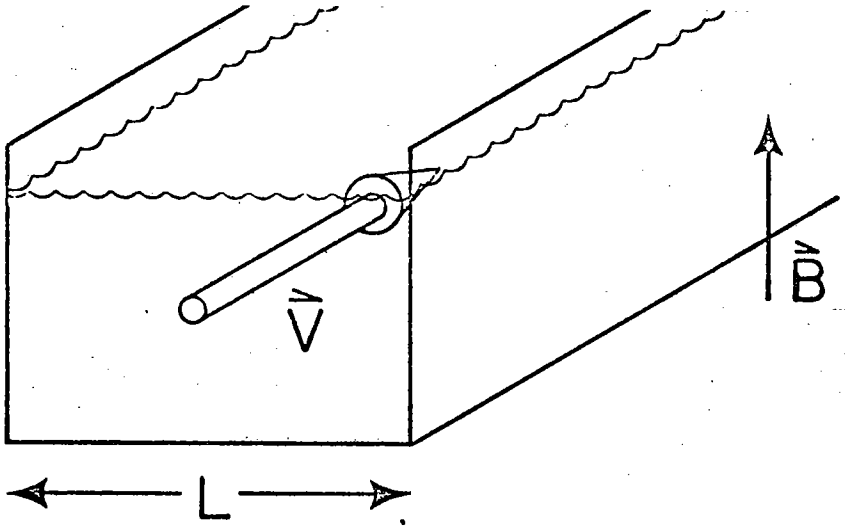

Figure 2. Uniform stream of sea water in an infinitly long trough

analysis the walls of the trough will be assumed to be first a perfect insulator (case 1), and second a perfect conductor (case 2).

In the first case the stationary potentiometer will measure the potential difference of VBL since no electric current flows. The potentiometer moving with the current will measure zero because electrostatic charges balance out the motional electric field. In the

second case the stationary potentiometer will measure zero because a current will flow in the walls of the trough reducing the potential between them to zero. The voltage produced by this current is measured by the moving potentiometer and is equal to -VBL.

If we now assume a horizontal ocean current of rectangular cross section extending uniformly to the ocean bottom, and of width L, flowing with a constant velocity $\vec{V}$ perpendicular to the earth's magnetic field $\vec{B}$, it would produce effects similar to those associated with the previously mentioned conducting trough containing sea water moving at a constant velocity $\vec{V}$. As the current flowed it would generate a constant emf proportional to VBL. The circuit would be closed through the rest of the water which is not in motion, and the bottom sediments. A circuit analogy for this flow is pictured in Figure 3. The emf and the segment of moving water have been replaced by a voltage source E_M and a resistance R_L, the return circuit of motionless water and bottom sediments by resistances R_B and R_H respectively.

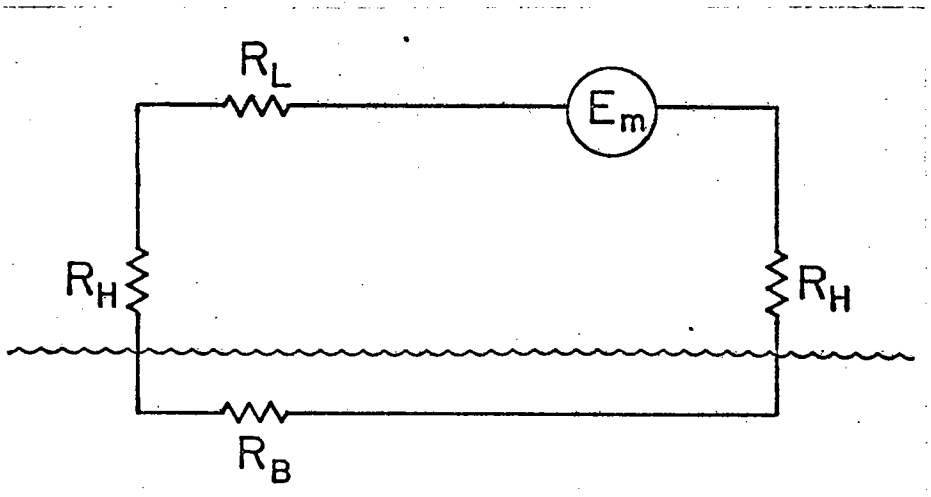

Figure 3. Circuit analogy for a uniform ocean moving in a magnetic field

In general, however, the flow in the ocean does not extend to the bottom uniformly. It is structured with the maximum current velocities more or less confined to the upper layers and the return circuit consists not only of the bottom sediments but also the fairly large section of semi-motionless sea water beneath the flow. The circuit analogy for this general case is pictured in Figure 4. The single voltage source E_M and resistors R_L and R_H have been replaced with arrays of N batteries and resistors.

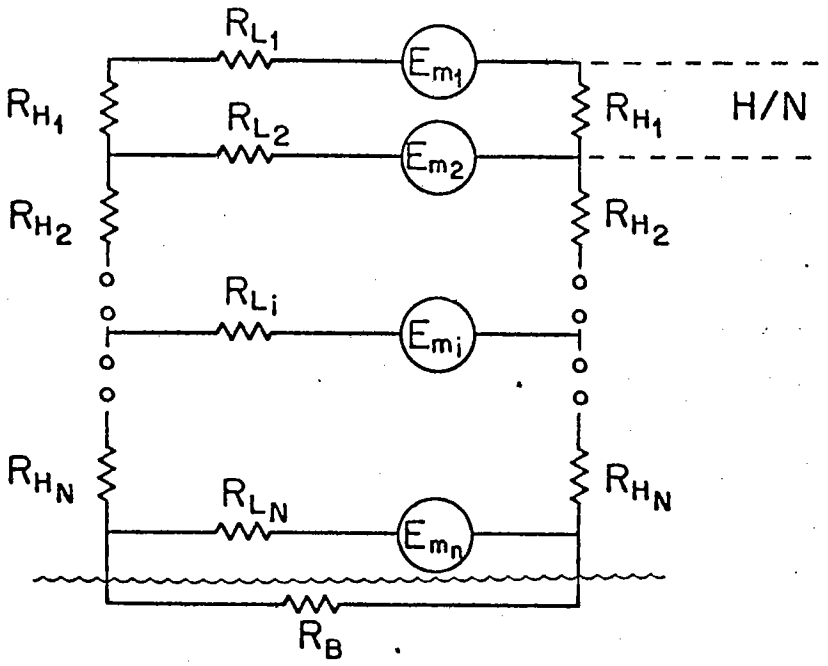

Figure 4. Circuit analogy for a stratified ocean moving in a magnetic field

The above circuit may be simplified if the total vertical resistance of the water column $\overline{R}_H$ is much less than the total horizontal resistance of the water column $\overline{R}_L$. The resistance $\overline{R}_L$ is approximately

$$\overline{R}_L \simeq \rho_w L/H \tag{13}$$

where ρ_w is the resistivity of the sea water. The resistance $\overline{R}_H$ is

approximately

$$\overline{R}_H = \rho_w H/L \tag{14}$$

therefore

$$\overline{R}_H/\overline{R}_L = (H/L)^2 \tag{15}$$

For a current like the Gulf Stream with an approximate width of 50 kilometers in a water depth of 5 kilometers, the above ratio is

$$\frac{\overline{R}_H}{\overline{R}_L} = \left(\frac{5km}{50km}\right)^2 = \frac{1}{100} \tag{16}$$

Therefore, $\overline{R}_H$ may be neglected for most work in large scale ocean currents.

The effect of the resistivity of the bottom can be better understood if we again consider an idealized ocean current of width L flowing with a constant velocity $\vec{V}$ extending uniformly to the ocean bottom. Let the depth of the water be designated as H, and the resistivity of the water and ocean bottom be ρ_w and ρ_b respectively; and assumed uniform. The resistance of the sea water can be approximated by

$$R_L \simeq \rho_w L/H \tag{17}$$

It is further assumed that the electric current extends down into the sea floor to a distance approximately equal to the stream width L.[2] Therefore, the bottom resistance is

$$R_B \simeq \rho_b L/L = \rho_b \tag{18}$$

The equivalent circuit for this case is pictured in Figure 5.

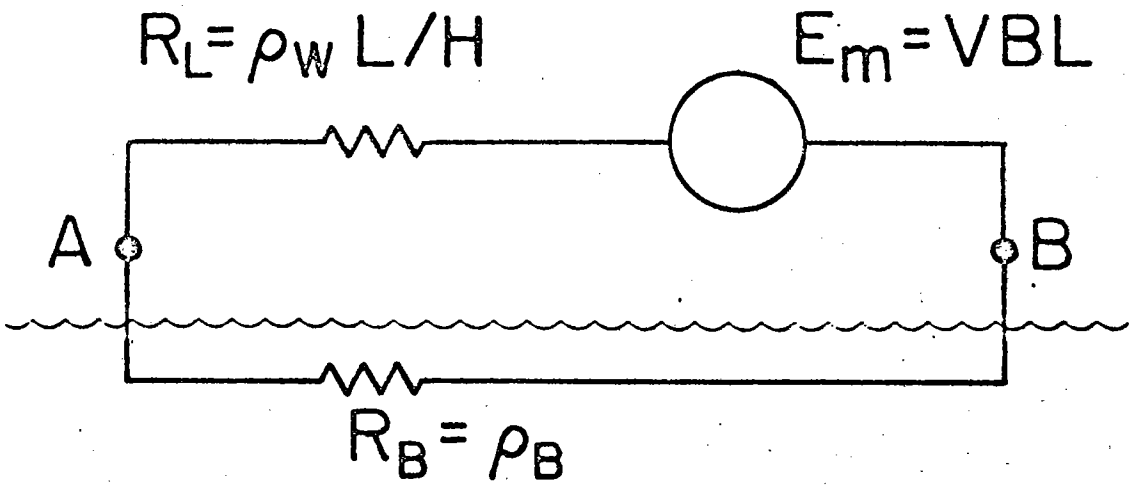

Figure 5. Circuit analogy for a uniform ocean moving in a magnetic field neglecting $\overline{R}_H$

Since the current I in the circuit is

$$I = E_M/(R_L + R_B) \tag{19}$$

the potential difference between points A and B is then

$$\phi_A - \phi_B = IR_B = \frac{E_M}{1+R_L/R_B} \tag{20}$$

or in terms of the physical parameters equation 20 becomes

$$\phi_A - \phi_B = \frac{VBL}{1+\rho_w/\rho_b(L/H)} \tag{21}$$

From equation 21 we can then see that the resistivity effects the measured potential by the ratio ρ_w/ρ_b. This ratio can vary between unity and 2.5×10^{-5}.[3] For a current such as the Gulf Stream, L/H is approximately 10. Thus, the potential gradient can vary greatly depending on the extent of the flow, depth of the water, and the

resistivity of the bottom sediments. But, for the deep ocean, particularly in the area of narrow currents, the effect of the sea floor can be ignored.

The effect of the vertical variations of the velocity structure must also be taken into consideration. Since the velocity profile in the ocean varies continuously with depth (see Figure 6), N should approach infinity. The strength of the individual batteries E_{M_i} will now be $V_i BL$ where V_i is the flow at the i^{th} level. Assuming that the sea water conductivity is constant with depth, each

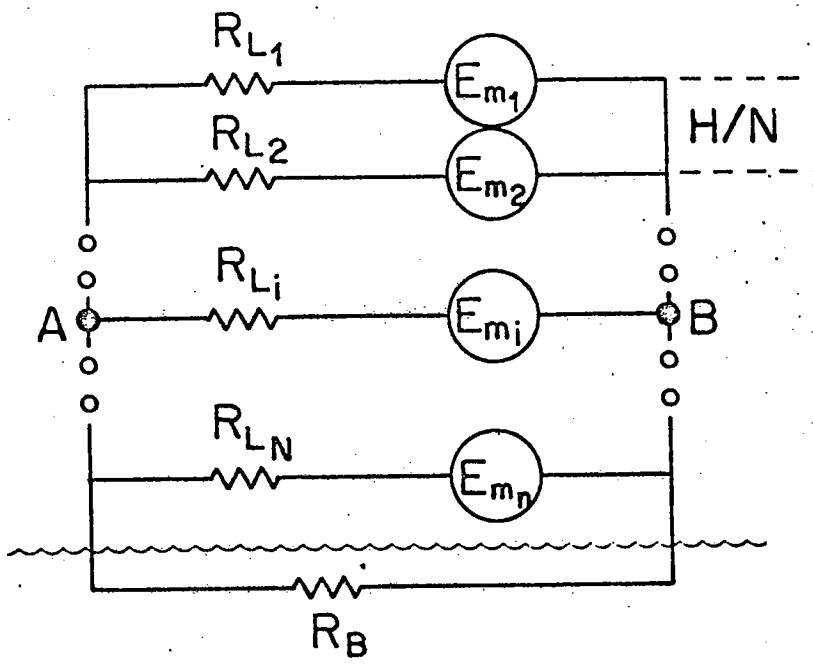

Figure 6. Circuit analogy for a stratified ocean moving in a magnetic field neglecting $\bar{R}_H$

resistor R_{L_i} will have a resistance of $\rho_w LN/H$ as N approaches infinity. Since $\phi_A - \phi_B$ is the potential difference between points A and B, the current flowing in each level I_i will be given by

$$I_i = \frac{[(\phi_A - \phi_B) - V_i BL]H}{\rho_w LN} \qquad (22)$$

The total current I in the N levels is then

$$I = \frac{1}{\rho_w L} \sum_{i=N}^{1} [(\phi_A - \phi_B) - V_i BL] \frac{H}{L} \qquad (23)$$

or going to a continuous function of depth,

$$I = \frac{H}{\rho_w L} [(\phi_A - \phi_B) - \frac{BL}{H} \int_{-H}^{o} V(z)\,dz] \qquad (24)$$

$$I = \frac{H}{\rho_w L} [(\phi_A - \phi_B) - \bar{V}BL] \qquad (25)$$

where $\bar{V}$ is the vertically averaged velocity and is equal to

$$\bar{V} = \frac{1}{H} \int_{-H}^{o} V(z)\,dz \qquad (26)$$

The circuit analogy in Figure 6 can now be simplified to that shown in Figure 7. Therefore, the current I is

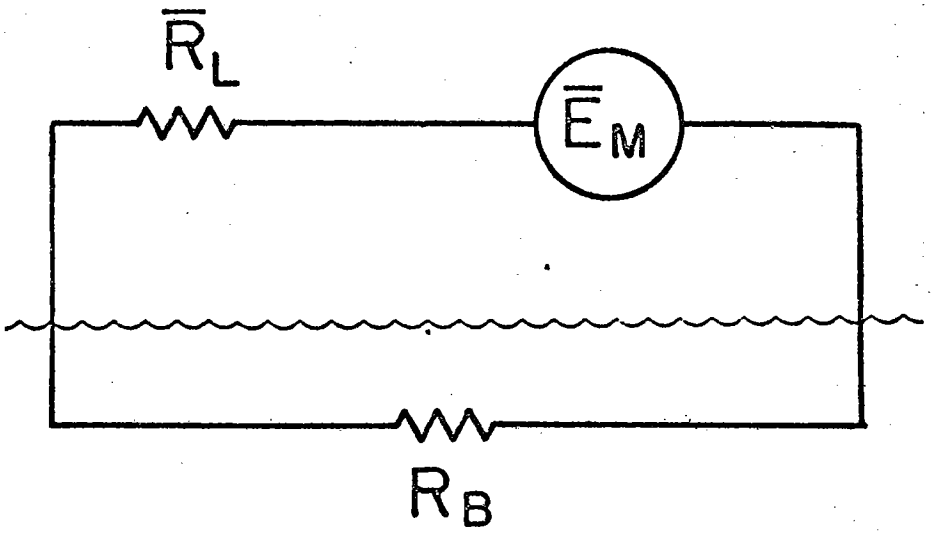

Figure 7. Equivalent circuit ocean current in Figure 6

$$I = \frac{\overline{E}_M}{\overline{R}_L + R_B} \qquad (27)$$

and the potential difference between pointa A and B is then

$$(\phi_A - \phi_B) = IR_B = \frac{\overline{E}_M}{1 + \overline{R}_L/R_B} \qquad (28)$$

For ocean currents where the flow is confined to the near surface waters, the voltage sources, as depicted in Figure 6, in the lower layers of the water column, will be of zero order.

III. Actual Electric Field Measurements

Figure 8 shows a ship moving with velocity $\vec{V}_s$ with respect to the water and towing a GEK. $\vec{V}$ is the velocity of the water with respect to the earth at the level of the instrument.

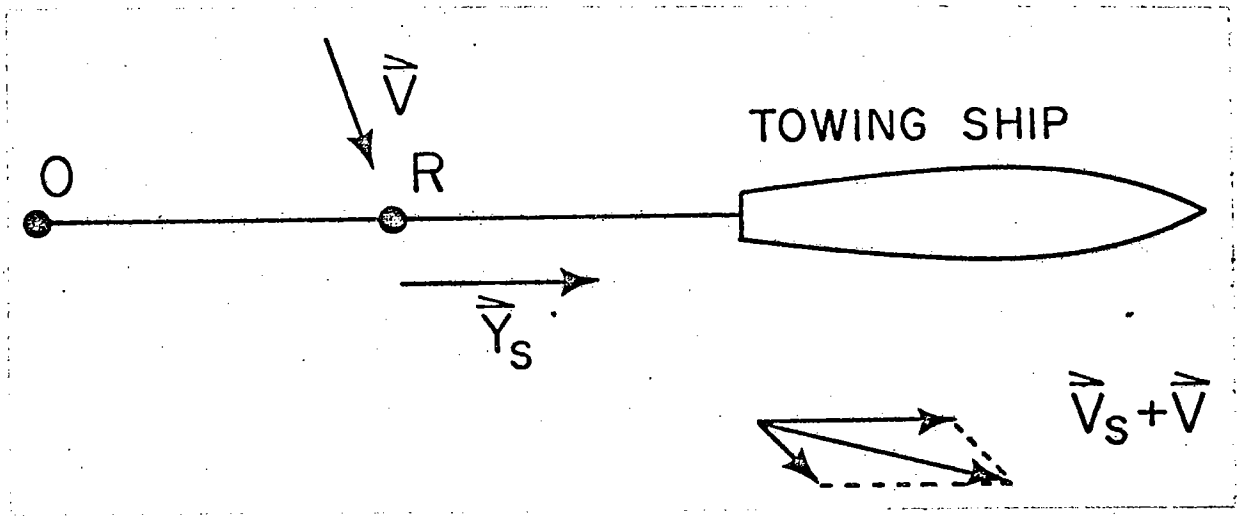

Figure 8. Towed electric field meter

The distance $\overline{OR}$ can either be an interelectrode distance as in earlier GEK's or the length of a salt bridge, in later models. The

absolute velocity of the segment $\overline{OR}$, in the absence of sideways disturbances, is

$$\vec{V}_{\overline{OR}} = \vec{V}_s + \vec{V} \tag{29}$$

The potential measured between the two points O and R will consist of two terms; the potential in the sea water $\nabla\phi \cdot \overline{OR}$, and the voltage induced in $\overline{OR}$ by virtue of its motion through the magnetic field of the earth $[(\vec{V}_s + \vec{V}) \times \vec{F}] \cdot \overline{OR}$ such that

$$(\text{Voltage})_{\text{measured}} = [\nabla\phi - (\vec{V}_s + \vec{V}) \times \vec{F}] \cdot \overline{OR} \tag{30}$$

If $(\vec{V}_s \times \vec{F})$ is assumed to be perpendicular to $\overline{OR}$ there will be no contribution from this term. Therefore

$$(\text{Voltage})_{\text{measured}} = (\nabla\phi - \vec{V} \times \vec{F}) \cdot \overline{OR} \tag{31}$$

This equation simply shows that the measured voltage is independent of the towing velocity of the ship as long as there are no horizontal excursions in $\overline{OR}$ and dependent on the potential in the sea water and its velocity. In terms of the measured electric field this becomes

$$\vec{E}_{\text{measured}} = \nabla\phi - \vec{V} \times \vec{F} \tag{32}$$

Values of $\vec{F}$, the earth's magnetic field, are readily available from the literature and if the components of $\nabla\phi$ were known, $\vec{V}$ could be found by measuring the potential difference between O and R on two different ship headings and transforming these vectors to determine $\vec{V}$, the horizontal current velocity vector. However $\nabla\phi$, the gradient

of electrostatic potential in the sea, is not initially known and so the measured voltage, and hence the desired current cannot be calculated.

From the earliest GEK operations it became necessary to cope with the lack of knowledge about the value of the potential gradient, $\nabla\phi$, in the sea in order to calculate current velocities. Thus, it became expedient to define a "K" factor which is simply the ratio of the desired or expected signal $(\vec{V} \times \vec{F})$ to the actual signal measured $[(\vec{V} \times \vec{F}) - \nabla\phi]$.[4]

$$K = \frac{|\overline{V} \times \overline{F}|}{|(\overline{V} \times \overline{F}) - \nabla\phi|} \tag{33}$$

Since $\nabla\phi$ roughly depends on the ratio of the sea water to bottom resistivities, the width of the current and the depth of the water, the K factor for a particular area of the sea was either estimated from a knowledge of these factors or calculated from the ratio of water speeds observed by other current measuring devices. Von Arx (1950) has estimated that the average value of K for the open sea is 1.04, where as on the continental shelf it averages less than 2.0, and in shoal water it may range from 1.5 to 15.0.[5] Once a K factor had been decided upon for a particular set of data, the signal received and hence the calculated velocity was then scaled up by a factor of K to give its "true" value.

Recently, Sanford (1971) has analytically solved for the quasi-static electric field in the sea for an idealized model of the ocean and earth. His analysis shows that in an ocean current which is broad compared with the ocean's depth, the potential gradient is

independent of depth and a function of $\overline{V}_H$, the vertically-averaged horizontal velocity in the entire water column. The horizontal components of the potential gradient in the sea are given by

$$\frac{\partial \phi}{\partial x} = F_z \overline{V}^*_y \tag{34}$$

$$\frac{\partial \phi}{\partial y} = F_z \overline{V}^*_x \tag{35}$$

where $\overline{V}^*$ is the vertically-averaged conductivity weighted velocity given by

$$\overline{\vec{V}}^* = \frac{1}{D(1+\alpha)} \int_{-D}^{o} \overline{V}_H dz \tag{36}$$

and

D = depth of water

$\overline{V}_H = (V_x, V_y, 0)$

α = ratio of the conductance of the bottom sediments to that of the ocean

Then, recalling that

$$\vec{E}_{measured} = \nabla\phi - \vec{V} \times \vec{F} \tag{37}$$

it follows that the horizontal components of $\vec{E}$ measured are

$$E_{measured\ x} = - F_z(V_y - \overline{V}^*_y) \tag{38}$$

$$E_{measured\ y} = F_z(V_x - \overline{V}^*_y) \tag{39}$$

These expressions state that if the x and y components of the measured electric field are found the horizontal components of the absolute water velocity V_x and V_y, at any given level, can be

calculated if $\bar{V}_x^*$ and $\bar{V}_y^*$, the conductivity weighted vertically averaged components of horizontal velocity, are known.

Since the K factor previously defined by von Arx is an empirically determined aid to the interpretation of data obtained by GEK methods, Sanford recommends that the use of the K factor be discontinued and that the GEK data "...should be interpreted as the vector difference between the surface and the vertically averaged velocities."[6]

And, $\bar{V}_x^*$ and $\bar{V}_y^*$ can be measured. Consider a bottom mounted electric field meter and assume for simplicity that the local current velocity is zero. Then since

$$V_x = 0 \tag{40}$$

$$V_y = 0 \tag{41}$$

the components of electric field measured by such an instrument would be

$$E_{\text{measured } x} = F_z \bar{V}_y^* \tag{42}$$

$$E_{\text{measured } y} = F_z \bar{V}_x^* \tag{43}$$

The local current velocity in the above mentioned case has been assumed to be zero but in general this is not always valid, therefore, a measurement of the local current velocity is desired. This measurement can be obtained by electro-magnetic means.

$$\frac{\partial \phi}{\partial x} = F_z V_y - J_x/\sigma \tag{44}$$

Between any two points in an undisturbed field

$$J_x/\sigma = F_z(V_y - \bar{V}_y) \tag{45}$$

with the introduction of a measuring instrument equation 45 is generally more complex due to the interference caused by the measuring instrument. Therefore,

$$J_x/\sigma = F_z(\alpha V_y - \beta \bar{V}_y) \tag{46}$$

where α and β are constants that can be obtained from the geometry of the problem. Substitution of equation 46 into equation 45 then yields

$$\frac{\partial \phi}{\partial x} = F_z V_y - F_z(\alpha V_y - \beta \bar{V}_y) \tag{47}$$

or

$$\frac{\partial \phi}{\partial x} = -F_z(\gamma V_y - \beta \bar{V}_y) \tag{48}$$

where $\gamma = \alpha - 1$

If the measuring instrument is an insulating cylinder, it can easily be shown that $\alpha = 2$ and $\gamma = 1$ if the voltage is measured on the skin of the instrument.

Therefore,

$$\frac{\partial \phi}{\partial x} = F_z \bar{V}_y \qquad \text{at infinity} \tag{49}$$

$$\frac{\partial \phi}{\partial x} = F_z(V_y - 2\bar{V}_y) \qquad \text{on instrument skin} \tag{50}$$

$$\frac{\partial \phi}{\partial x} = F_z(\gamma V_y - \beta \bar{V}_y) \qquad \text{in general} \tag{51}$$

Then, with the additional measurement of $\partial\phi/\partial z$ and if the measuring instrument aligns itself with the local velocity, V_x and V_y, the local velocity, can be obtained.

B. PREVIOUS EFFORTS IN ELECTRIC FIELD MEASUREMENTS

Michael Faraday, in 1832, predicted the presence of induced electric fields in sea water. Faraday later attempted to detect the induced electric currents created by the flow of the Thames River, but his attempt failed. The chemical potentials, due to a metal-electrode junction between the copper electrodes and the river water, masked his predicted results.

Electromagnetic effects were later observed on long lengths of broken telegraph cable after the middle of the 19th century. Young, Gerrard and Javons (1920) measured voltages induced by tidal motions in Dartmouth Harbor by means of drifting and moored non-polarizing electrodes but their results were not utilized until 1946 in oceanographic research because of instrumentation problems.[7] Von Arx (1950) developed a surface-towed Geomagnetic Electro-Kinetograph and applied the electromagnetic method to observations in shoal water, including both observations while underway and at a fixed station. Further measurements using submarine cables have been made by Stommel (1954) and Runcorn (1964).

Recently Drever and Sanford (1970) have developed a free-fall GEK which is capable of rapidly measuring the variations of horizontal velocity as a function of depth with a precision better than 1 cm/sec. The essential difference between this instrument and the surface towed GEK is that the former is used at the sea surface to study the horizontal structure of an ocean current while the free-fall instrument is used to study the vertical structure. The main objective for developing the free-fall instrument was to determine if it was

feasible to measure the weak motionally induced electric fields in the ocean currents. Results have shown that it was not only practical but very useful oceanographically to make these measurements.

Williams et al (1971) have developed a new type of towed surface GEK which is the first prototype of a bottom mounted GEK. In previous electromagnetic current meters a serious problem has been the determination of the offset potential of the electrodes in the sea water. Williams has solved this problem by a unique valve switching mechanism between the ends of the salt bridge and the electrodes.

Theoretical studies, necessary for interpreting the measurements in terms of water movements, have been made by Stommel (1948) and Longuet-Higgins (1949). Malkus and Stern (1952) have proved some important integral theorems. Most recently Sanford (1971) has extended the theory of Longuet-Higgins et al (1954) to three-dimensional time-dependent currents in a laterally unbounded ocean of nonuniform depth. To include mutual induction between the ocean and the mantel, an idealized model of the earth's electric conductivity was used by Sanford.

C. BOTTOM MOUNTED ELECTRIC FIELD METER (PROTOTYPE)

A towed surface instrument which was the first prototype for the bottom mounted electric field meter was constructed and tested during the summer of 1971 (Williams et al 1971). A salt bridge used in conjunction with a valve switching arrangement permitted the induced electromotive force and the electrode offset potential to be easily determined. Extensive laboratory tests and several field experiments proved the reliability and effectiveness of the design. Field tests included towing the instrument at the ocean surface as well as bottom deployment in shallow water.

A schematic diagram of the valve switching arrangement is depicted in Figure 9. A solenoid operated water switch, 1, which is normally closed separates the electrodes. Switch 2 is normally open. In this "normal" configuration the potential is measured between

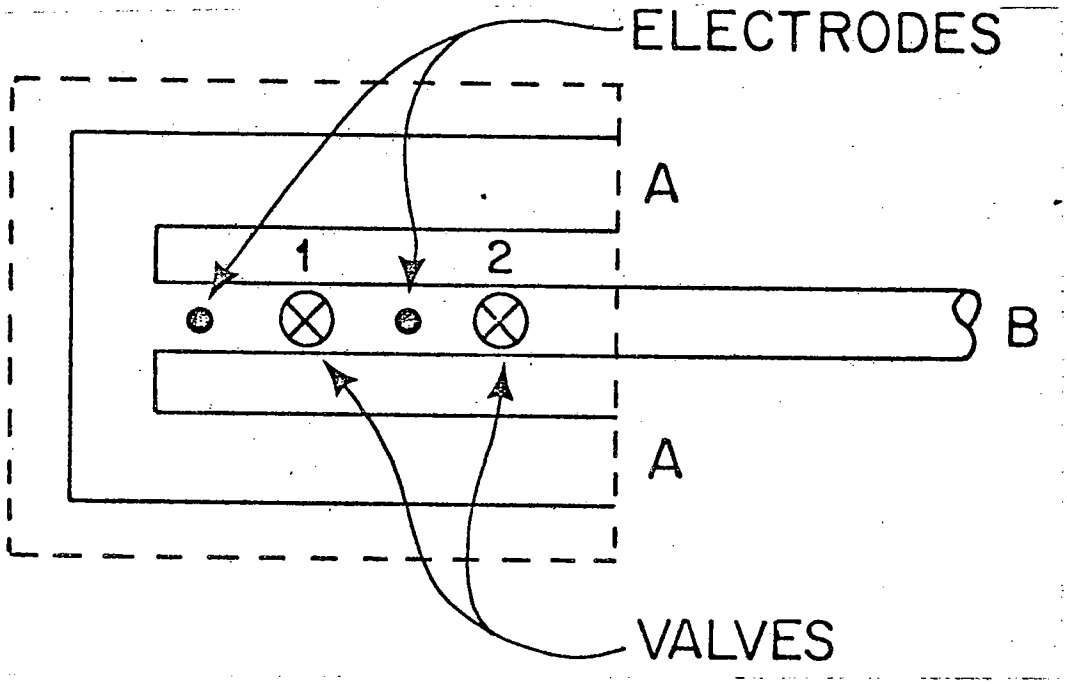

Figure 9. Schematic diagram of the valve switching arrangement - prototype

points A (near the unit) and point B (at the far end of the salt bridge). When switch 1 is opened and switch 2 is closed the electrodes then see a sea water short circuit and thus the electrode offset potential is measured. In the electrode manifold the electrodes have been placed in close proximity to each other in order to minimize the temperature and salinity differences between them.

The salt bridge for the electrodes consists of sea water-filled tygon tubes. Modular lengths were used to allow damaged pieces to be replaced easily and variable lengths to be deployed. The salt bridge has low impedance through the sea water path along its length and very high impedance across the walls of the tygon tubes and at the electrodes therefore there is little voltage drop along its extent. The induced EMF measured by the electrodes is amplified within the instrument before it is transmitted by cable for recording and evaluation aboard the support vessel.

A serious problem that was encountered with the prototype instrument was the existence of ground loops: when an electrical path was present through the electrodes to ground and back to the electrodes through a sea water path, a significant electrical current passed through the electrodes and caused considerable drift in the electrode potential. In order to avoid all possibility of ground loops and to permit total portable support all power supplies were replaced by batteries.

Numerous field tests were held to check out the prototype in the towed configuration as well as bottom deployments. The valve switching worked perfectly on all deployments. Of specific interest to this

report are the bottom deployments especially the one conducted at Gate of Canso at Woods Hole, Massachusetts. This test site was selected because of its accessibility and high currents (see Figure 10). The GEK was anchored on the bottom in approximately 15 feet of water, and a 30 meter salt bridge was stretched across the channel

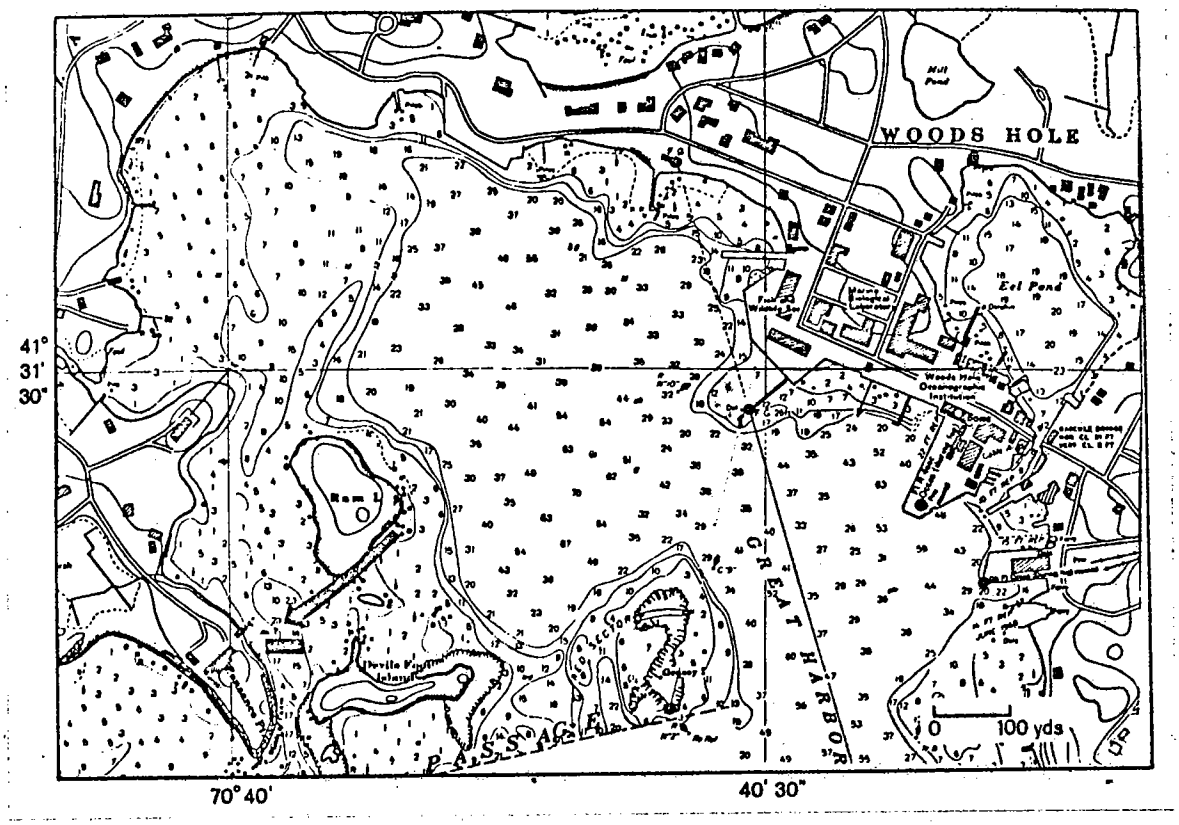

Figure 10. Bottom deployment site - prototype

under a region of significant current flow. The average signal strength, at the test site, varied between 100 and 200 microvolts. The conversion of this raw data, $\overline{V}^{*}XB$, in microvolts, to current, in knots, yielded an average flow of .26 to .52 knots. This flow did

not agree with the expected flow: it was anticipated that a much higher flow would be observed. An independent measurement of current in the area indicated surface currents in excess of 4 knots at times.

A complete analysis of the electrical currents flowing in the Gate of Canso depends on the exact velocity distribution, bottom conductivity and bathymetry. It is not intended here to do such an analysis but rather to derive an approximate conversion from measured voltage to velocity through the gate. This will be done so that the reader may observe the procedure that one must use at times to convert raw data to a usuable form. To simplify the calculation two models will be used; the first to express the geometry in the simplest way and the second to simplify the field calculation.

The simplest parameters which can be assumed for the Gate of Canso are the width of the channel, the depth of the water, and the average velocity of the water. Therefore, let us represent the Gate as a rectangular channel of infinite length, width L, and depth H. Let the channel be filled with water of resistivity ρ_w moving at a uniform velocity V normal to a vertical magnetic field B. The bottom has a uniform resistivity ρ_B and is presumed to extend to infinity (see Figure 11).

We wish to find the voltage between the lower corners as a function of the velocity. In the idealization of the Gate that has been assumed, there is a distribution of potential along the sides and bottom of the channel which arises from the geomagnetic electrokinetic field and from the electric current distribution in the sediment and the water. A great simplification can be made by

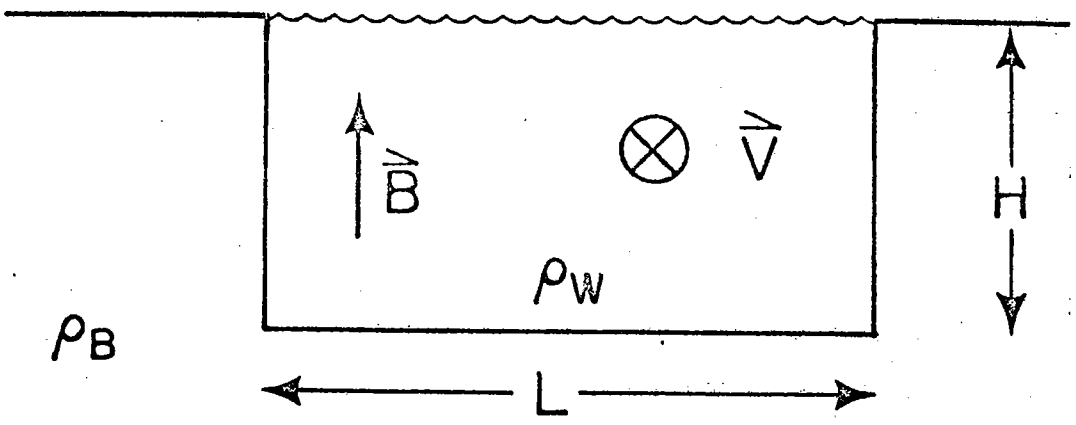

Figure 11. Gate of Canso - geometry approximation

assuming the side walls of the channel are conducting cylinders half immersed in the sediment, and the water in the channel is replaced by an emf, $\vec{E} = \vec{V}X\vec{B}$ in series with a resistance $R_w = \rho_w L/H$ per unit length. This model is easy to solve and is an approximation to the first model if the dimensions are chosen suitably. A schematic configuration of a unit length of this second model is shown in Figure 12.

To scale the second model to the first, the immersed circumference of the cylinders is made equal to the depth of the channel plus a portion of the bottom width, 1/4L. Thus, $r_o = (H+L/4)\pi$. It can be noted that the resistance through the sediment between C and D is just twice what it would be between two full cylinders of radius r_o separated by L in a full space of sediment with resistivity ρ_B.

The full cylinders in a full space of sediment are symmetric and the resistance per unit length between them can be calculated.

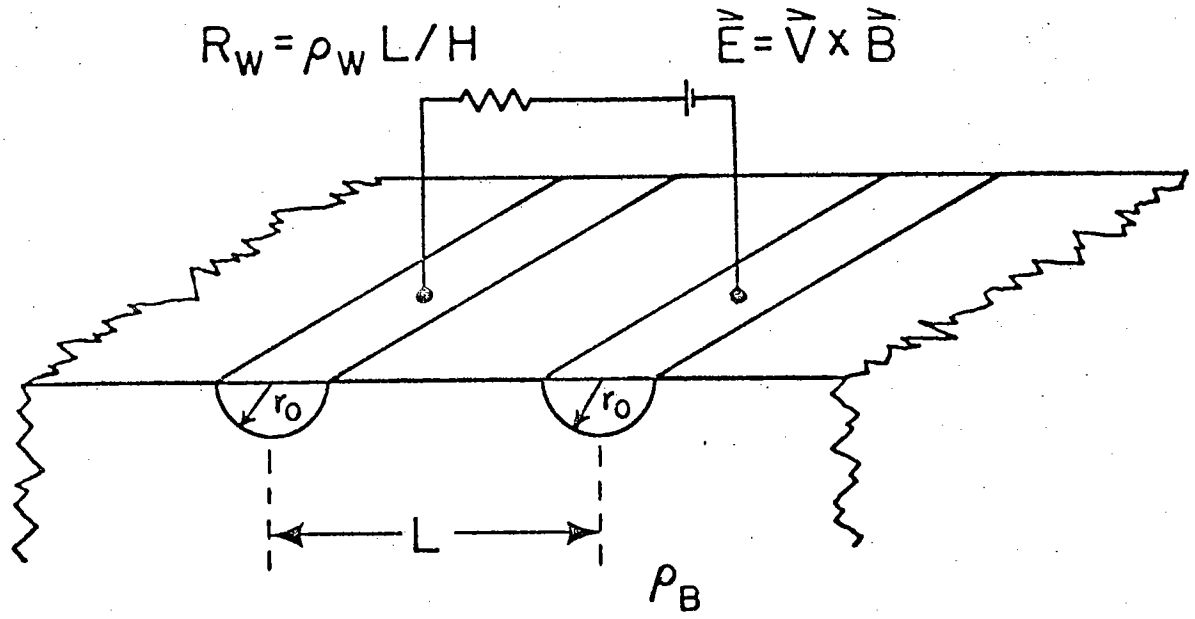

Figure 12. Gate of Canso - field calculation approximation

Assuming that $L >> r_o$

$$R_{\text{full space}} \simeq 2\rho_B \int_{r_o}^{L} 1/2\pi r dr \tag{52}$$

then,

$$R_B = 2R_{\text{full space}} \simeq 2\left[\frac{\rho_B}{\pi} LN(L/r_o)\right] \tag{53}$$

and finally

$$R_B = \frac{2\rho_B}{\pi} Ln[\pi L/(H+L/4)] \tag{54}$$

Then, the voltage across the channel will be

$$E_M = ER_B/(R_B+R_W) \tag{55}$$

At the Gate of Canso L = 30 meters, H = 5 meters, and $\rho_B \simeq 4\rho_W$. Therefore

$$R_B = 1.3\rho_B = 5.2\rho_w \tag{56}$$

$$R_w = 6.0\rho_w \tag{57}$$

$$E_M = .46E \tag{58}$$

Hence, 1/2 of our voltage drop occurs in the sediment. This value can then be included in the expression for measured voltage as a K factor such that

$$[K]E_{measured} = \overline{V}^* XB, \text{ where } K = 2 \tag{59}$$

Assuming a 100 microvolt signal, it follows that

$$E = 100 \times 10^{-6} \text{volts}/30 \text{ meters} \tag{60}$$

$$E = 3.33 \times 10^{-6} \text{volts/meter} \tag{61}$$

and

$$\overline{V}^* = \frac{(2)(3.33\times10^{-6}\text{volts/meter})}{.5\times10^{-4}\text{webers/meter}} \tag{62}$$

$$\overline{V}^* \tilde{=} .26 \text{ knots} \tag{63}$$

As stated previously the current near the surface, measured independently was in excess of 4 knots at times. The vertically averaged current at the Gate of Canso is on the order of 1/4 to 1/2 knot. This difference can be explained if; (A) the assumptions in the above mentioned analysis are in error, or (B) the average flow through the Gate is, indeed, between 1/4 and 1/2 knot and our original assumptions concerning this flow are in error.

The assumptions used in the analysis appear to be good. Malkus and Stern (1952) used the same approximations with good results. Therefore, it appears that the assumption concerning the flow is in error. It was assumed that the current was approximately uniform throughout the depth of the channel in the vicinity of the deployed GEK. It is now believed that there is only a tongue of current that moves through the gate with relatively quiet water and countercurrents in other regions.

D. OVERALL DESCRIPTION OF THE DESIGNED BOTTOM MOUNTED ELECTRIC FIELD METER

The general external configuration of the bottom mounted electric field meter is shown in Figure 13. The main housing for the instrument is a 20 5/8 inch diameter cylinder approximately 8 feet in length. This external skin is constructed out of 1/4 inch thick, medium density, polyethylene. This is the same type of outer skin that Drever and Sanford (1971) used on their free-fall electric field meter. The purpose of this cylinder is not for strength but rather for protection against unwanted self induced fields generated by metalic substances within the shell. The bottom of the outer covering is open to the sea water, but the top is sealed as well as possible so that a long range dipole field is not set up. The outer shell is divided into two halves to facilitate assembly. This break in the skin is sealed with a 19 1/4 inch diameter latex band. This band also releases entrained air in the instrument as it sinks below the surface. Holes are provided in the upper half of the skin covered by the latex band for the release of this air.

There are four separate measurements made of the electric field by the instrument. Measurements of the electric field are made in the x, y, and z directions by the series of horizontal arms near the top of the instrument. The arms in the x-y plane are constructed from PVC Type II, Schedule 80, pipe. They have an inside diameter of 2 inches. The length of each of these salt bridges will be approximately 12 feet, but they can be adjusted in length by inserting tubes of differing length. Type II PVC is a high impact plastic and was

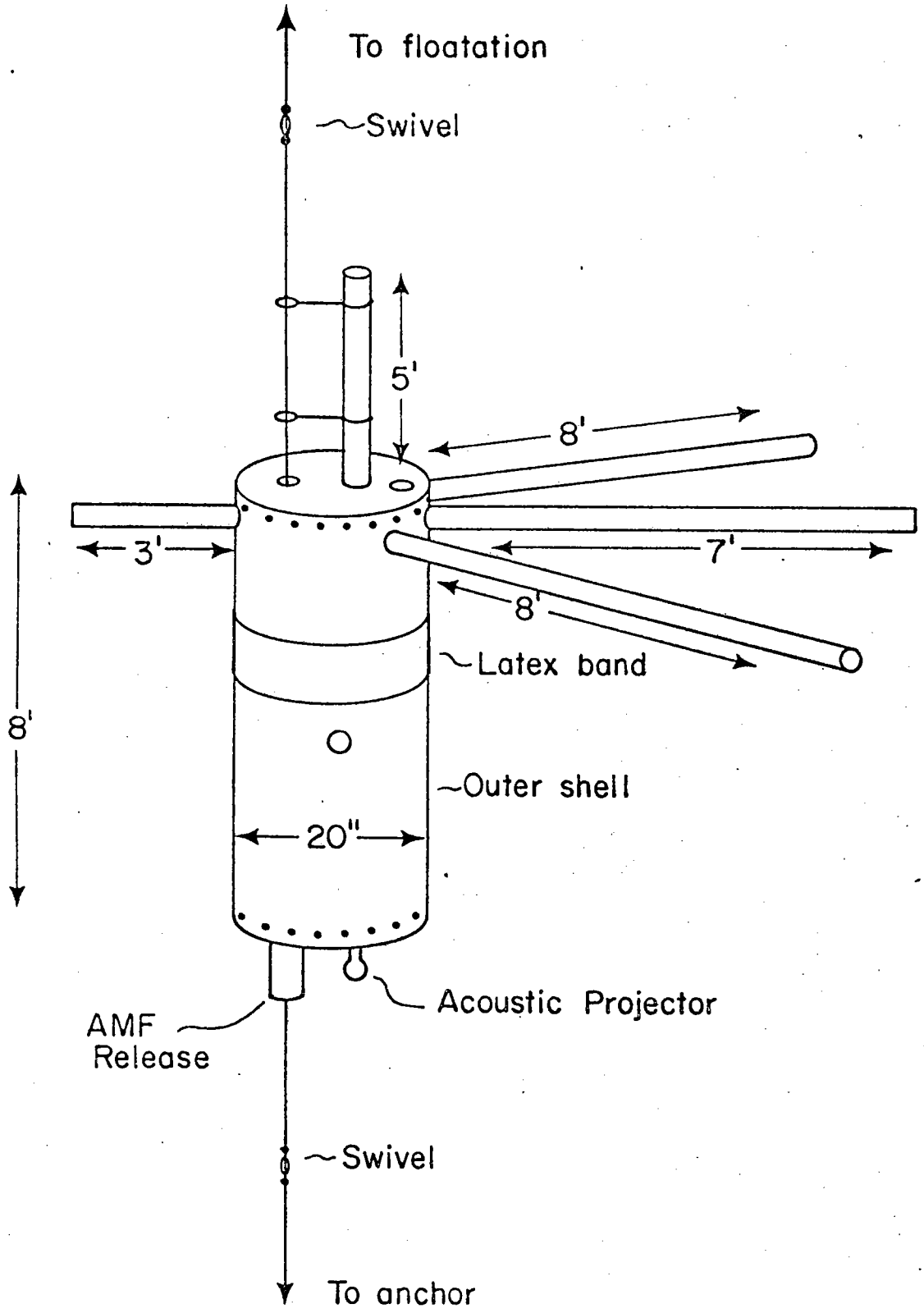

Figure 13. External configuration of the bottom mounted electric field meter

chosen in order that it might inhibit breakage and absorb energy during possible collisions with the support ship. If the arms do break, they can be easily and inexpensively replaced. The vertical salt bridge will be approximately 6 feet in length but, like the horizontal arms, it can be adjusted to any desirable length. This salt bridge will be constructed out of semi-flexible tygon tubing and will be lashed to the mooring line.

The fourth electric field measurement will be made on the skin of the cylindrical shell midway along its length. This salt bridge will run along the internal wall of the housing and be fabricated from 1 inch tygon tubing. This measurement allows the local water velocity to be computed. A compass will be mounted internally to monitor the instrument's orientation with north. Pressure will also be monitored.

A re-cockable AMF release and an acoustic projector are also visible in the picture of the external configuration of the bottom mounted electric field meter. Interrogation of the instrument is possible from the support ship through the AMF acoustic link. Release will generally be commanded through this link.

There are two swivels used in the unit when it is deployed with its own mooring. The swivels are used so that the instrument might be free to turn into the direction of the local current. The upper swivel is pressure compensated and will be recovered with the instrument. The lower swivel is packed with grease to exclude salt water. An inexpensive swivel is used as it will be left behind, along with the anchor, after the instrument releases from the bottom. The anchor is

a simple concrete block. The weight of the instrument, including the anchor, will be 150 lb. heavy in water.

The buoyancy for the instrument will be provided by 16 inch glass spheres. Each sphere supplies 48 pounds of buoyancy and has the capability of being used to 20,000 feet. The spheres will be individually attached to the mooring cable separated by at least a one-meter distance in order that if one of the spheres fails, sympathetic explosion of the others will not occur.

A cut away view showing the internal structure of the bottom mounted electric field meter is shown in Figure 14. Of principal interest in this figure are the arm support block, water switch housing, and dual end cap.

The arms of the instrument are supported by a 4 inch long, 20 inch diameter, polypropylene cylinder. The supported length of the arms of the unit is approximately 5 1/2 inches. The electrical seals for the salt bridges are provided by O-rings. The arms are first screwed into the polypropylene support, engaging the O-ring seals, and then secured in place by jam nuts. The salt bridge is continued to the water switch housing by semi-flexible, 3/4 inch inside diameter, tygon tubing.

The water switch housing is constructed out of 16 inch diameter, 3/16 inch thick, PVC cylindrical shell. The unit is oil filled and is pressure compensated. The seal at the top of the water switch housing is provided by an O-ring. The bottom of the unit contains the pressure compensating membrane. This membrane also provides a static seal.

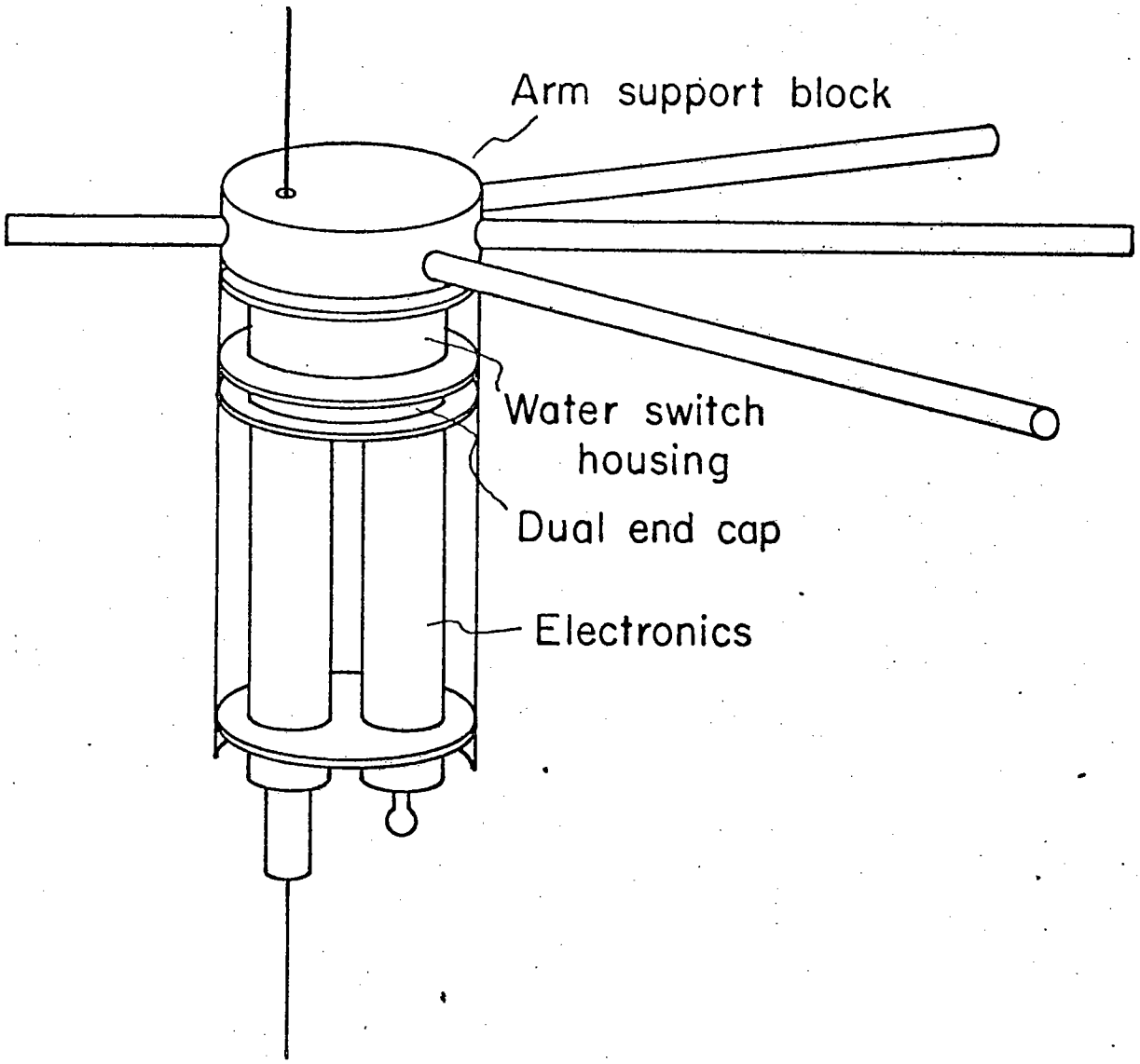

Figure 14. Internal configuration of the bottom mounted electric field meter

The electronics for the instrument are housed in two 7 1/2 inch, outside diameter, 7075-T6, aluminum tubes. The dual top endcap connects the two cylinders electrically. Within the endcap there are two 3/4 inch interconnections with the electric sections. These have been provided so that wires can pass freely between the two electronic sections.

E. Specific Description of the Designed Bottom Electric Field Meter

I. Optimum Configuration of the Salt Bridges and Cylinder Diameter

The potential in the vicinity of an insulating infinite circular cylinder introduced into a previously uniform electrostatic field of intensity E_o is given by

$$\phi(r, \theta) = -E_o[1 + \frac{a^2}{r^2}]r \cos\theta \qquad (64)$$

where a is the radius of the cylinder (see Figure 15).

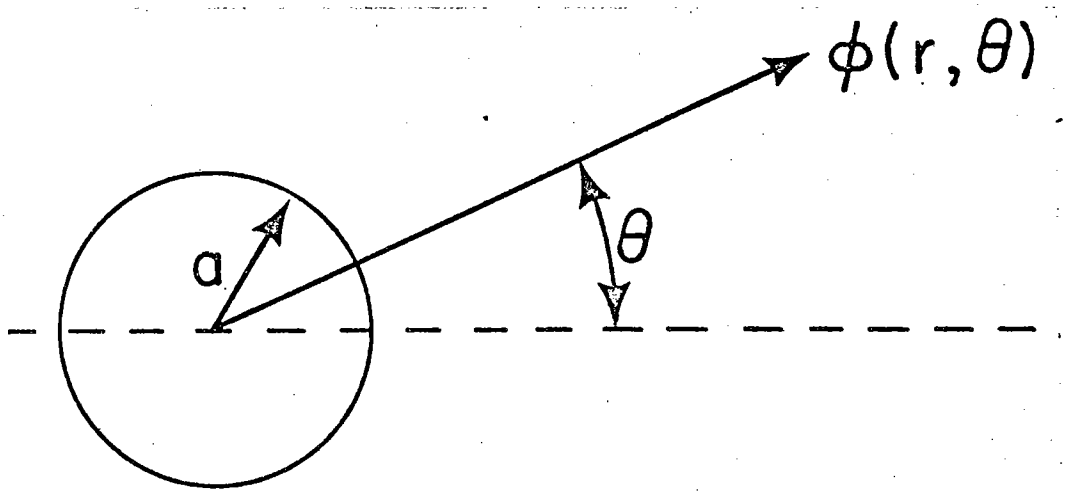

Figure 15. Circular cylinder - general

Of interest to this report is the potential between two points in this field of intensity E_o. Let ϕ_1 and ϕ_2 be two such points such that

$$-\phi_1 = E_o \frac{a^2}{r_1} \cos\theta_1 + E_o r_1 \cos\theta_1 \qquad (65)$$

$$-\phi_2 = E_o \frac{a^2}{r_2} \cos\theta_2 + E_o r_2 \cos\theta_2 \qquad (66)$$

then

$$\phi_2 - \phi_1 = \left[E_o \frac{a^2}{r_1} \cos\theta_1 - E_o \frac{a^2}{r_2} \cos\theta_2\right] + \left[E_o r_1 \cos\theta_1 + E_o r_2 \cos\theta_2\right] \qquad (67)$$

Two cases will now be looked at. First we will assume that $\cos\theta_1 = -\cos\theta_2$ (See Figure 16)

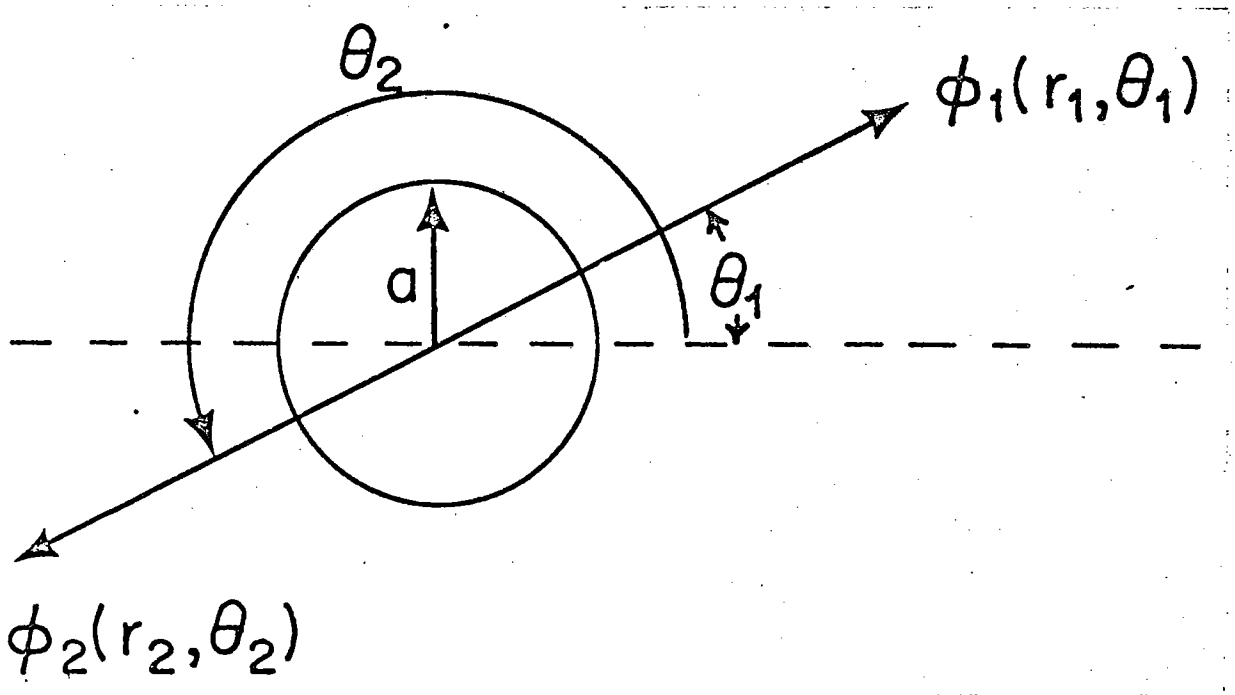

Figure 16. Circular cylinder - $\cos\theta_1 = \cos\theta_2$, $r_1 \neq r_2$

Using the above assumption equation 67 then becomes

$$\phi_2 - \phi_1 = E_o a^2 \cos\theta_1 \left(\frac{1}{r_1} + \frac{1}{r_2}\right) + E_o \cos\theta_1 (r_2 + r_1) \tag{68}$$

where the desired measurement is

$$E_o \cos\theta_1 (r_2 + r_1) \tag{69}$$

and the error that is introduced due to the cylinder is

$$E_o \cos\theta_1 \left(\frac{1}{r_1} + \frac{1}{r_2}\right) \tag{70}$$

Then the ratio of the introduced signal to the desired signal is

$$\frac{\text{introduced}}{\text{desired}} = \frac{E_o a^2 \cos\theta_1 \left(\frac{1}{r_1} + \frac{1}{r_2}\right)}{E_o \cos\theta_1 (r_1 + r_2)} \tag{71}$$

or

$$\frac{\text{introduced}}{\text{desired}} = a^2 \left(\frac{1}{r_1 r_2}\right) \tag{72}$$

From the above result it can be noted that the magnitude of the ratio is independent of the angle θ and increases as the second power of the radius of the cylinder a.

The second case to be considered assumes that $r_1 = r_2$ and that $\cos\theta_1 \neq \cos\theta_2$ (See Figure 17).

Using the above assumptions equation 67 then becomes

$$\phi_2 - \phi_1 = E_o \frac{a^2}{r} (\cos\theta_1 - \cos\theta_2) + E_o r (\cos\theta_1 - \cos\theta_2) \tag{73}$$

and the ratio of the introduced signal to the desired signal is

$$\frac{\text{introduced}}{\text{desired}} = \frac{E_o \frac{a^2}{r} (\cos\theta_1 - \cos\theta_2)}{E_o r (\cos\theta_1 - \cos\theta_2)} \tag{74}$$

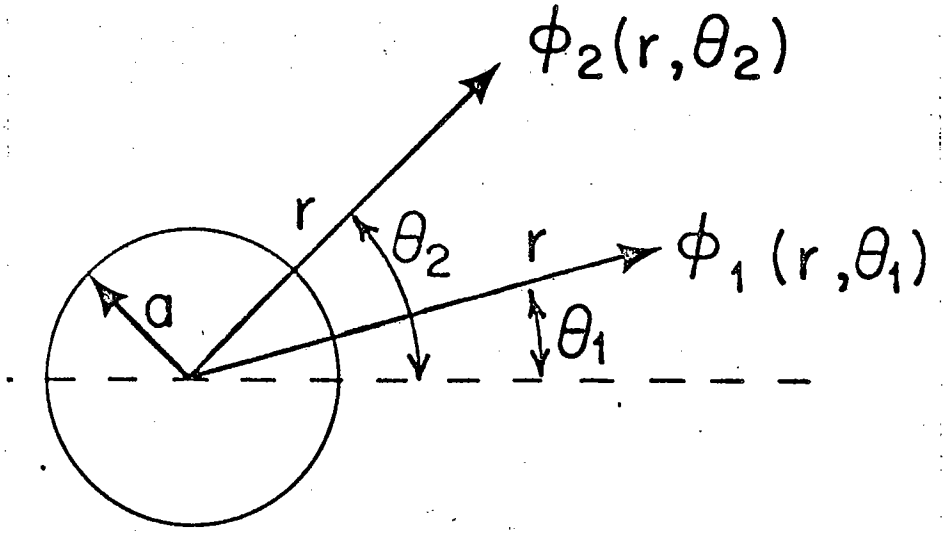

Figure 17. Circular cylinder - $\cos\theta_1 \neq \cos\theta_2$, $r_1 = r_2$

or

$$\frac{\text{introduced}}{\text{desired}} = \frac{a^2}{r^2} \tag{75}$$

The magnitude of the error is again independent of θ and varies as the square of the radius of the cylinder and the inverse square of the arm length.

From the above calculations it should then be noted that the diameter of the cylindrical body of the instrument should be as small as possible and the distance between ϕ_1 and ϕ_2 should be as great as possible so that the introduced error be as small as possible.

The controlling factor in the bottom mounted electric field meter's cylindrical shell is the size of the housing for the unit's water switch. The minimum diameter needed for the chamber is 15 inches but with the housing included the diameter is extended to 17

inches. In order that there be room for the frame assembly a cylinder diameter of 20 inches has been chosen. When this value for the diameter is substituted into equation 72 and 75 they become, respectively

$$\%\text{error} = \frac{a^2}{r_1 r_2}(100) = \frac{69.4}{r_1 r_2} \tag{76}$$

$$\%\text{error} = \frac{a^2}{r^2}(100) = \frac{69.4}{r^2} \tag{77}$$

The configuration for the arms in the xy plane was chosen to produce a length between ϕ_1 and ϕ_2 of 12 feet and also to minimize the problem of handling the unit during deployment and recovery, as well as maximize its ability to orient itself with bottom currents in the vicinity of the unit (See Figure 18).

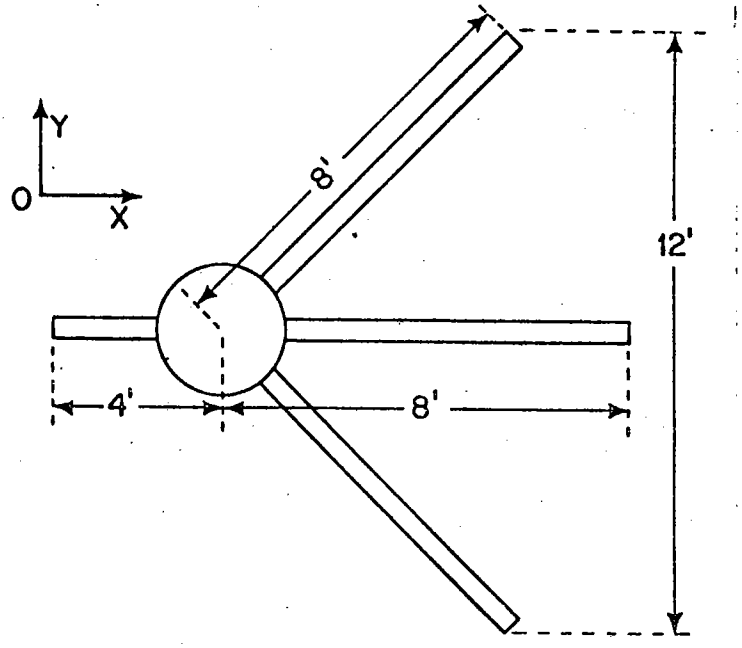

Figure 18. General arm configuration

then, equations 76 and 77 become, respectively

$$\%\text{error} = \frac{69.4}{(4)\ (8)} \simeq 2.2\% \tag{78}$$

$$\%\text{error} = \frac{69.4}{(8)\ (8)} \simeq 1.1\% \tag{79}$$

Consideration has also been given to the placement of the arms on the instrument in the vertical plane. Should they be placed in the middle of the instrument or at the extremes, the top or bottom of the instrument? Sanford (private communication) has approximated the case of a semi-infinite cylinder with a prolate spheroid and has shown that it would be more advantageous to place the arms at the top or bottom of the instrument. Ship board handling procedures will be easiest with arms at the top of the instrument.

II. Design of the Salt Bridges

1) Arms

In the prototype electric field meter a tygon salt bridge was used, tens of meters in length. A suitable replacement for this bridge had to be found for the bottom mounted electric field meter. On the bottom mounted instrument the salt bridges will have to withstand the rigors of deployment and recovery as well as the free fall to the bottom. In order that the recorded signal be relatively free from errors the length of the salt bridge must be on the order of 12 feet. Further restrictions are that the arms be constructed from a non-metalic material and that the inside diameter of the arms be on the order of 2 inches.

Different arm designs were considered all of which could be placed into one of two different catagories; those that deployed after the

unit reached the bottom, and those that were already in place before the unit was placed in the water. The latter catagory was chosen for reliability and simplicity. Of specific interest then, because the arms will be in place before deployment, are the forces that the arms will encounter during the instrument's free fall to the ocean bottom.

The maximum drag forces on the instrument will be encountered when the unit reaches terminal velocity. Therefore, the total drag on the instrument must equal the weight in water of the unit.

$$\text{weight in water} = \text{drag (anchor, instrument arms, instrument case, glass floats)} \tag{80}$$

An estimate of 1 meter/second for the terminal velocity will be assumed for selection of drag coefficients and weight in water will be 150 pounds. Let the component parts of the instrument be as shown in Figure 19.

Then,

$$C_D \text{ arms} \approx .98$$

$$C_D \text{ spheres} \approx .5$$

$$C_D \text{ cylinder} \approx .9$$

$$C_D \text{ anchor} \approx 1.2$$

The drag force is given by

$$\text{drag} = 1/2\rho SV^2 C_D \tag{81}$$

Substitution into equations 80 and 81, and solving for the terminal velocity V, yield

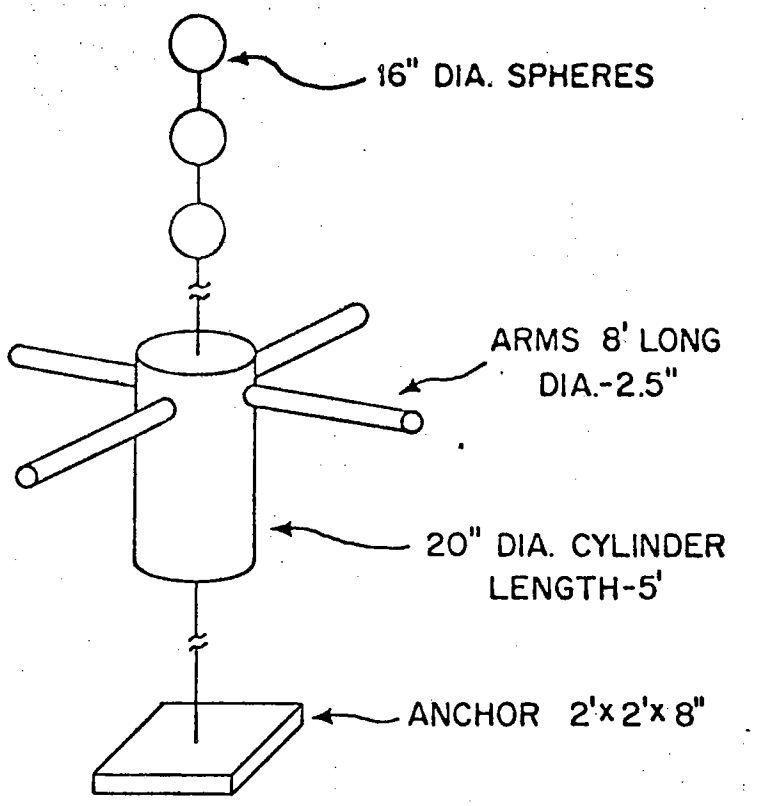

Figure 19. Basic geometry of bottom mounted electric field meter

$$V = 3.12 \text{ft/sec} = .95 \text{ M/sec} \qquad (82)$$

Since insulating arms are required, plastics were considered. Poly-vinyl chloride and polypropylene are readily available in standard pipe sizes therefore an analysis was conducted to determine the suitability of arms constructed from these materials. The analysis consisted of determining the maximum shear, bending moment, deflection and stress of various pipe sizes in air and stationary on the ocean bottom, as well as during the unit's critical free fall to

the bottom. The arm designs that were considered were one piece construction, two piece construction, and multidiameter construction (See Appendix B for detailed design of the arms).

One further constraint was placed on the decision of what pipe size should be used in the final design of the bottom mounted electric field meter: the electrical resistance of sea water. The impedance of the salt bridge must be less than 5,000 ohms. A graph of resistance, in ohms per centimeter, versus inside diameter of pipe, in inches, is shown in Figure 20.

The final design for the salt bridges uses 2 inch PVC, Type II, Schedule 80, pipe. The PVC material was chosen instead of the polyproplyene because of its greater strength and impact resistance. A single unsupported length of pipe was selected; a single piece to lower the replacement cost, unsupported because supports could alter the potential field in the vicinity of the instrument. (See Appendix B).

2) The Water Switch

The valve switching mechanism for the bottom electric field meter was one of the earliest design problems encountered. The valve switching for the prototype instrument in which 1/4 inch surgical tubing was pinched shut worked extremely well. Since there were no major problems with this approach it was decided that further development of this design would be a first course of action.

A test was conducted to determine how much force is needed to close off the 1/4 inch inside diameter surgical tubing. The inner surface of the tubing was coated with a thin film of silicon grease

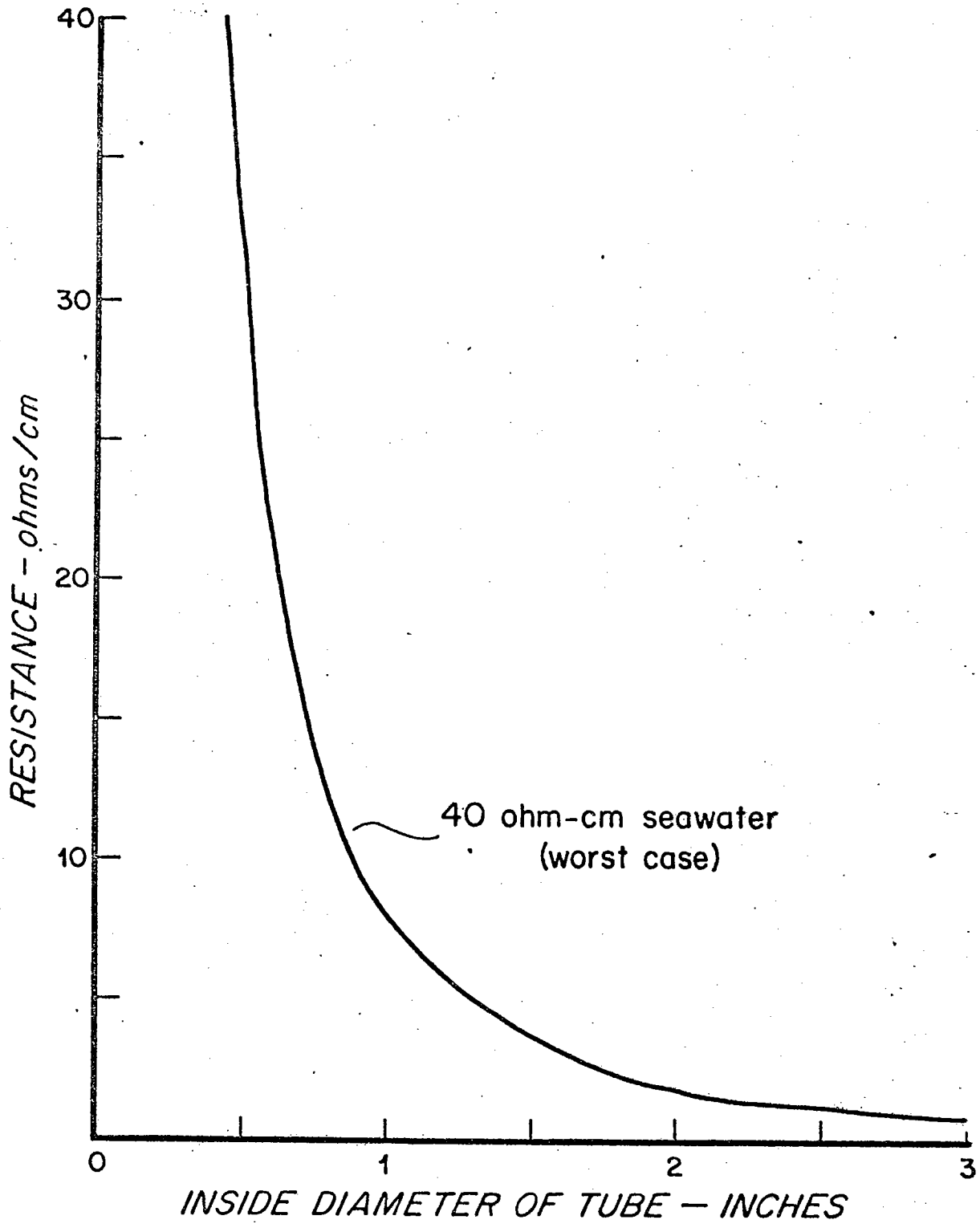

Figure 20. Resistance versus diameter of pipe

to improve the electrical close off. The results of this test are plotted as force in ounces, versus deflection of the inner diameter in inches (See Figure 21). From the graph it can be seen that the force required to close the tubes is approximately 22 ounces.

There are four salt bridges needed for the bottom mounted electric field meter and because of this there is the requirement that either eight or sixteen tubes must be used, depending on whether or not the offset will be recorded and later subtracted from the signal or eliminated from the measurement by means of mechanical switching. The later case is the desired one, if possible, but it is the one that requires sixteen tubes. A simple analysis, described below, was conducted to see if the sixteen tube method was practical.

If the mechanical switching method is used, eight tubes must be opened and eight tubes must be closed silmultaneously. The tubes can be modeled as springs, each with a spring constant K. If the opened and closed tubes are connected in parallel, as depicted in Figure 22, the equivalent K, K_{eq}, assuming that all K's are equal, becomes

$$K_{eq} = \sum_{i=i}^{N} K_i = 8K \qquad (83)$$

and the external force F required for a displacement δ from the base line is given by

$$F = 16\delta K \qquad (84)$$

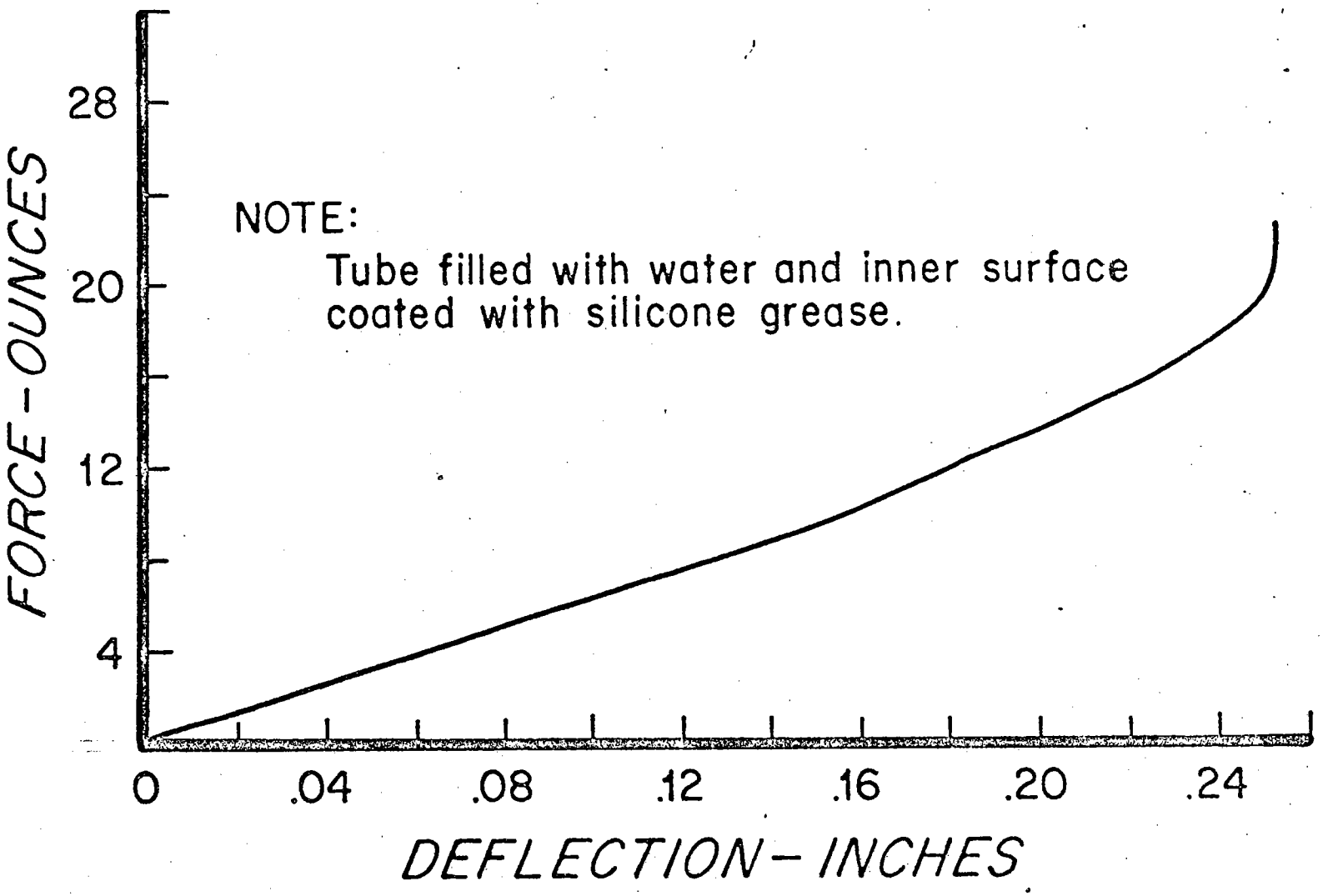

Figure 21. Force required versus deflection of the inner diameter

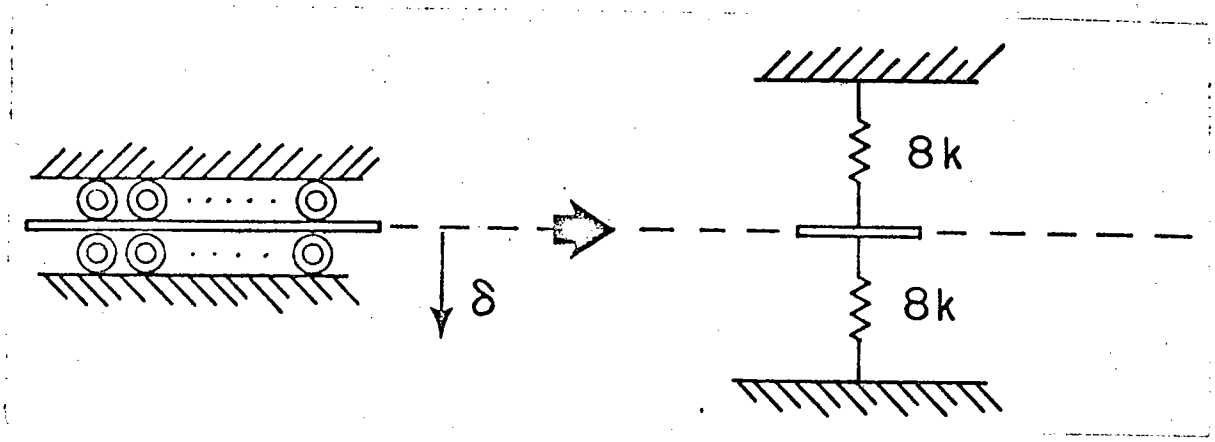

Figure 22. Spring analogy for tubes connected in parallel

If the opened and closed tubes are connected in series as shown in Figure 23, the equivalent K, again assuming that all K's are equal, becomes

$$\frac{1}{K_{eq}} = \sum_{i=i}^{N} \frac{1}{K_i} \tag{85}$$

$$K_{eq} = 1/8K \tag{86}$$

It should be noted that the deflection must now be 8 times as great as the parallel analysis. The external force required for a displacement 8δ is then given by

$$F = 2\delta K \tag{87}$$

The displacement δ is from a partially closed position to complete closure. The partial closure position was chosen to be .175 inches,

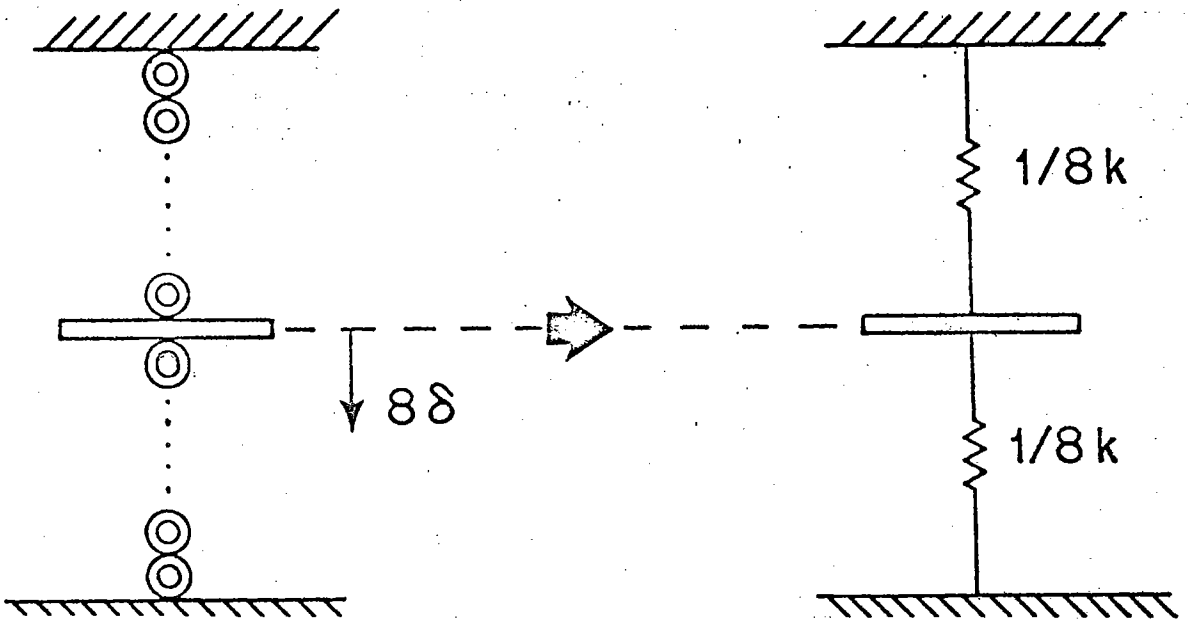

Figure 23. Spring analogy for tubes connected in series

therefore δ for this analysis is .0375 inches. The force required to close the tube to .175 inches is 12 ounces; the force required for electrical cut off is 22 ounces (See Figure 21). The spring constant K of the surgical tube is then

$$K = \frac{\Delta \text{force}}{\Delta \text{deflection}} = \frac{(22 - 12)\ \text{oz.}}{(.250 - .175)\text{in.}} \tag{88}$$

$$K = 133\ \text{oz./in.} \tag{89}$$

Therefore, if the tubes are connected in parallel the force required and throw T, become

$$F = (16)(.0375\ \text{in.})\left(133\frac{\text{oz.}}{\text{in.}}\right) = 80\ \text{oz.} \tag{90}$$

$$T = (2)(.0375\ \text{in.}) = .075\ \text{in.} \tag{91}$$

If the tubes are connected in series

$$F = (2)(.0375 \text{ in.})(133\tfrac{\text{oz.}}{\text{in.}}) = 10 \text{ oz.} \quad (92)$$

$$T = (16)(.0375 \text{ in.}) = .6 \text{ in.} \quad (93)$$

From these results we can see that if the tubes are connected in parallel the total throw is very small, but there is the hidden disadvantage that there is no guarantee that all of the tubes will close. If one tube has a slightly thicker wall thickness than the other tubes it would close first and block the remaining tubes from closing. Therefore, the series connected approach was deemed to be the superior method.

Another constraint, not present in the prototype bottom mounted electric field meter, will now be added to the analysis. The instrument must be able to remain on the bottom of the ocean for at least a one month duration, completely self sufficient. Because of this constraint a self locking mechanical switching network was desired. Power should only be needed to switch the circuit and then be turned off so that the power drain will be minimal. The final design selected is shown in Figure 24. Appendix A contains the detailed mechanical analysis of this circuit.

The three parts of Figure 24 show the toggling action of the water switch: A) shows the top row of tubes open and the bottom row closed, B) depicts the intermediate position and C) shows the top row of tubes closed and the bottom open. Each solenoid is energized for approximately 100 milliseconds only during the switching operation. The switch is self locking due to the mechanical advantage obtained by the geometry of the linkage of the water switch.

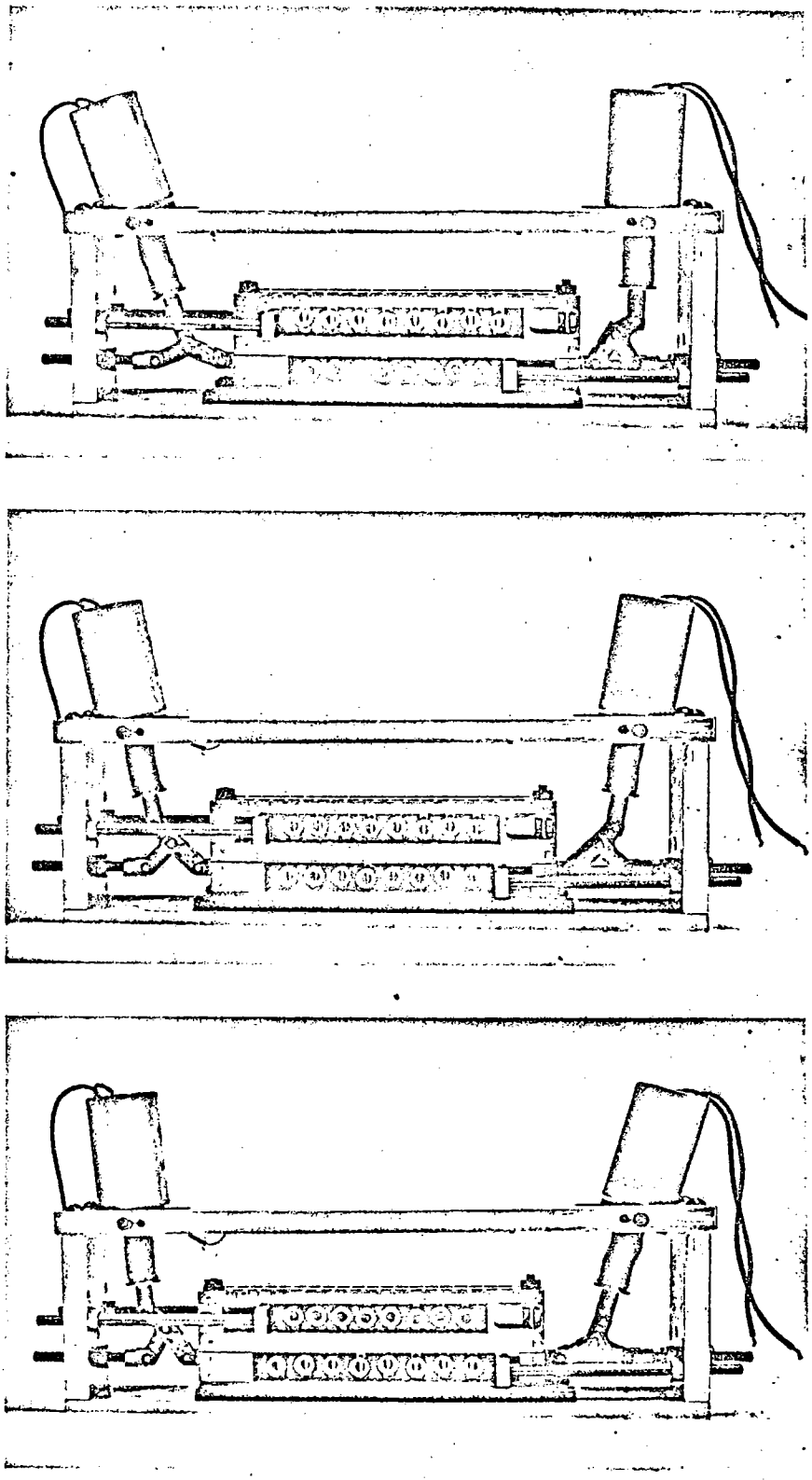

Figure 24. Water switch

(See Appendix A).

The guides that the shuttle of the water switch travel on, as well as the spacers between the tubes, are constructed from rulon so that frictional effects will be minimal.

3) The Electrode and Arm Manifolds

Pictures of the arm manifold and part of the electrode manifold can be seen in Figure 25. In the electrode manifold the electrodes are placed as close as possible to each other so that the temperature and salinity differences between them are minimized. The minimal spacing is critical in that a one degree centigrade temperature difference between a pair of electrodes will cause an offset voltage of about 350 microvolts between the electrodes; a salinity difference of one part per thousand in the water near each electrode causes a voltage difference of about 500 microvolts.[8] Thus, keeping the electrodes in close proximity, immersed in approximately the same water, reduces the offset potential between them.

The electrodes are connected to the electrode manifold by Swagelock connections. This is done in order that a seal be provided between the sea water, within the electrode chambers, and the pressure compensating fluid external to the manifold. All of the interconnections between the electrodes are completed inside of the manifold instead of externally in order to obtain a compact design. The schematic diagrams shown in Figure 26 A, B, and C depict how the internal plumbing provides for the switching of the electrodes.

In the configuration shown in Figure 26A electrode 1 is looking at point A and electrode 2 is looking at point B. If those switches

Arm Manifold

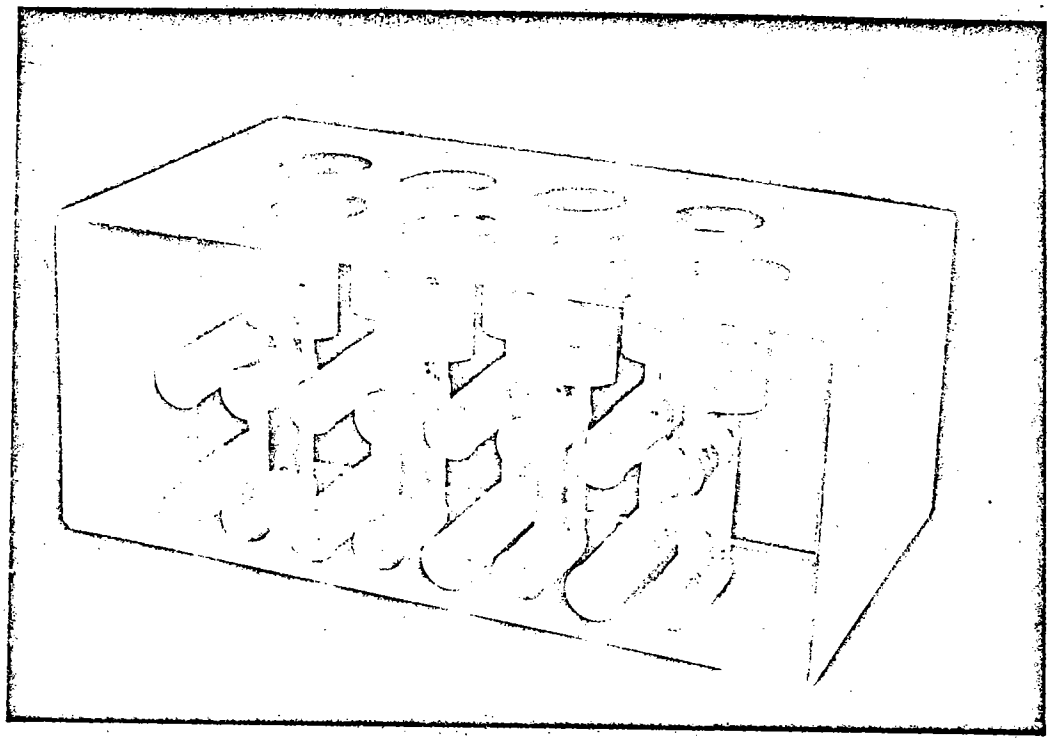

Electrode Manifold

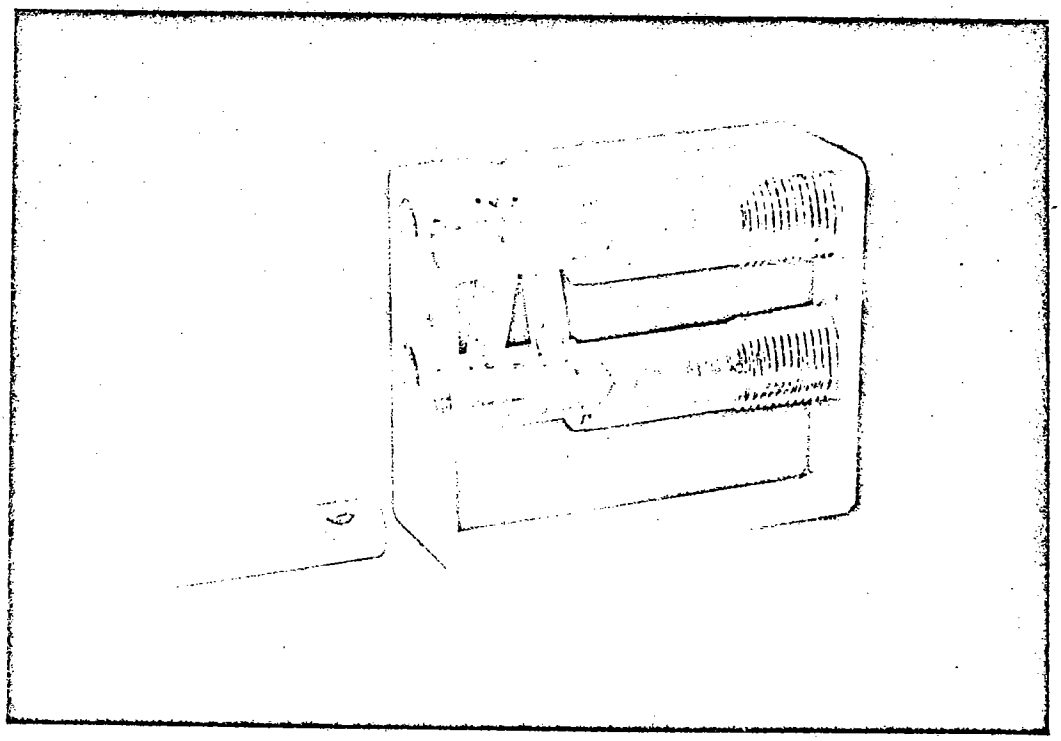

Figure 25

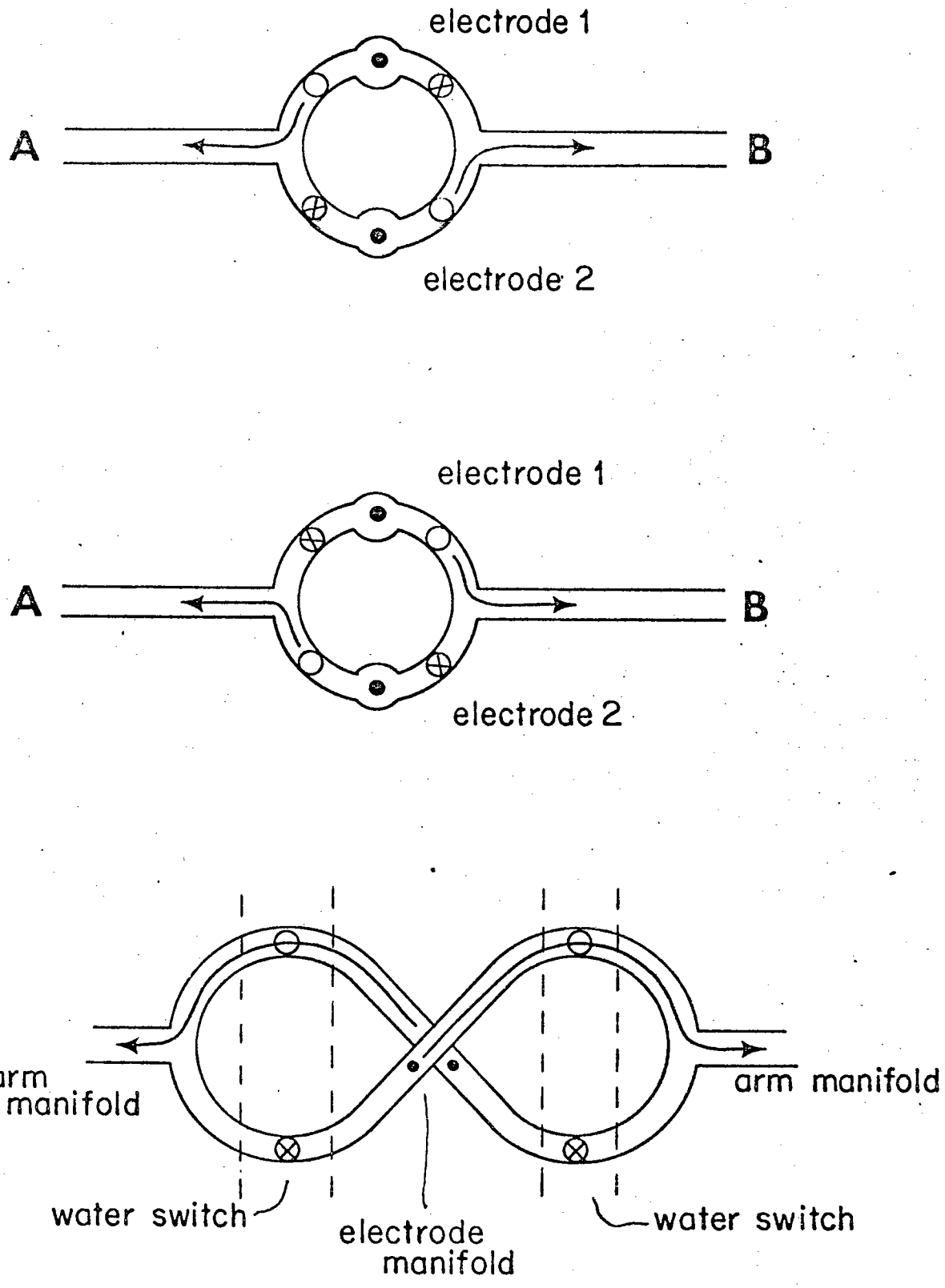

Figure 26. Schematic diagram of valve switching

that are closed then open, as shown in Figure 26B, and in like manner those that are open close, electrode 1 will then be looking at Point B and electrode 2 will now be looking at Point A. The water switch, previously described, provides the necessary switching.

In Figure 26C the configuration depicted in Figures 26A and B have been changed so that the reader may more easily decern the makeup of the arm and electrode manifolds. The manifolds are interconnected through the water switch by means of 1/4 inch, inside diameter tubing.

4) Electrodes

The electrodes for the bottom mounted electric field meter are basically the same as those used by von Arx in his first electric field meter. They are patterned after A.S. Keston's (1935) non-polarizing silver-silver bromide electrode.[9] The raw ingredients for the present electrodes are silver rod, silver wire gauze, silver chloride powder and silver oxide powder. A thick paste is prepared from the silver chloride, silver oxide and distilled water. The ratio of silver chloride to silver oxide is 9 to 1. The paste is then applied to the silver gauze and fired at a temperature of 450°C. This firing bonds the silver metal and the silver chloride. The silver oxide is decomposed in the process.[10]

It is of interest to note that since von Arx's first use of these silver-silver chloride electrodes there have been no major innovations to the electrodes. Recently, however, development of a replacement electrode using field effect transistors is currently being initiated (See Appendix C).

III. Front End Electronics

The electronics for the bottom mounted electric field meter have been, primarily, designed by Mr. Robert Drever of the Woods Hole Oceanographic Institution. It is not intended here to give a complete description of the complex electronics package but rather a brief description so that the reader will, in general, know what becomes of the measured signal. A block diagram of the front end electronics is given in Figure 27.

The maximum signal expected is ±200 microvolts riding on top of a maximum expected ±5 millivolt offset (see point A on Figure 28). Due to the valve switching mechanism, which in actuality is a chopper, the signal observed at point B appears as a modulated signal. The signal is then amplified by a double to single ended amplifier of high impedance. The impedance of the arms of the bottom mounted electric field will be on the order of 3KΩ. The mismatch between the arms of each salt bridge will be less than 200Ω.

After the signal is amplified it will be processed through a bandpass filter, .0016 Hz to 50.0 Hz. This filter, in essence, is a high pass filter and will allow the AC signal, data, to pass while blocking the DC, offset potential. This signal can be observed at point C. The signal is then processed by a voltage to frequency converter, 0 to 1 KHz output corresponding to a 0-5 volt input (see point D). The up-down counter and shift register performs the necessary integration of the signal. The integrated signal is then recorded on digital magnetic tape. The capacity of the recorder is approximately 10.6×10^6 bits of information.

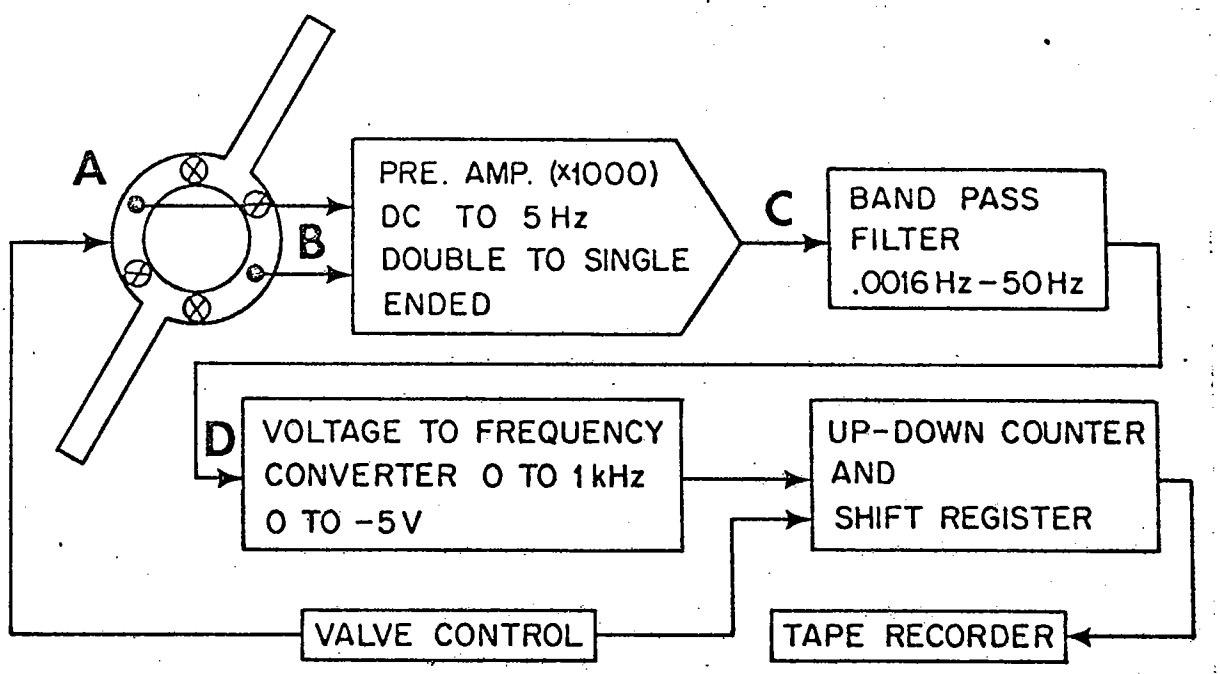

Figure 27. Front end electronics - block diagram

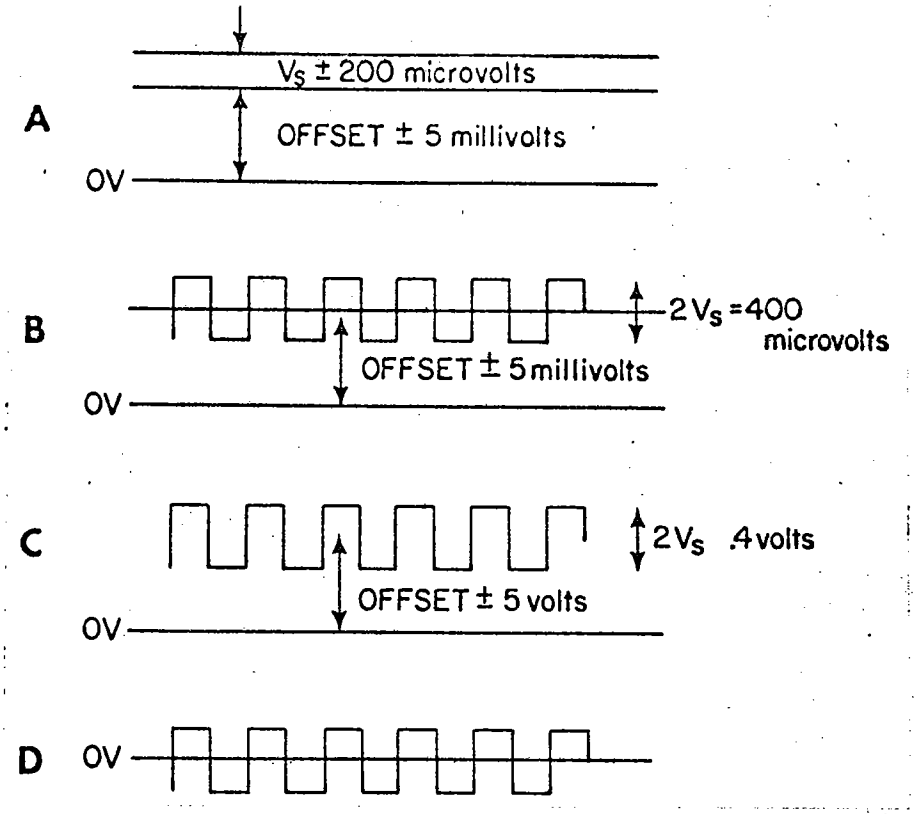

Figure 28. Front end electronics - signals

APPENDIX A

Detailed Design of the Water Switch

A detailed analysis of the mechanics and forces associated with the water switch is given below (See Figure 29). Given θ_1 and the force needed to hold the tubes closed, it is desired to find out what the throw of the solenoid must be and the force required to activate the shuttle.

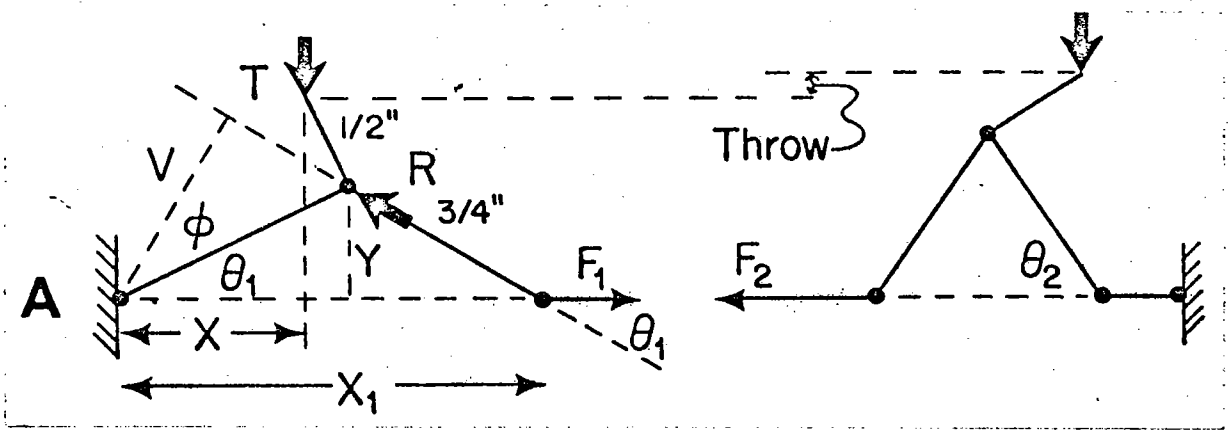

Figure 29. Schematic diagram of water switch

Taking moments about point A yields

$$T_x = RV$$

where

T = spring tension

$$x = \sqrt{(1/2)^2 + (3/4)^2}\cos(\theta_1+\phi)$$

$$V = 3/2 \cos\theta_1 \sin\theta_1$$

$$R = F_1/\cos\theta_1$$

then

$$T\sqrt{13/16} \cos(\theta_1+\phi) = [F_1/\cos\theta_1][3/2\cos\theta_1\sin\theta_1]$$

solving for F_1 yields

$$F_1 = \frac{(2/3)(13/16)^{1/2}\cos(\theta_1+\phi)}{\sin\theta_1} T_1$$

by similar analysis

$$F_2 = \frac{(2/3)(13/16)^{1/2}\cos(\theta_2+\phi)}{\sin\theta_2} T_2$$

where θ_2 is uniquely defined by θ_1.

Then, if T_1 and T_2 are assumed to be equal we have that

$$\frac{\sin\theta_1}{\cos(\theta_1+\phi)}F_1 = \frac{\sin\theta_2}{\cos(\theta_2+\phi)}F_2$$

since

$$\Delta F = F_1 - F_2$$

it follows that

$$F_1 = -\frac{\frac{\sin\theta_2}{\cos(\theta_2+\varphi)}}{[\frac{\sin\theta_1}{\cos(\theta_1+\phi)} - \frac{\sin\theta_2}{\cos(\theta_2+\phi)}]} \Delta F$$

$$F_2 = -\frac{\frac{\sin\theta_1}{\cos(\theta_1+\phi)}}{[\frac{\sin\theta_2}{\cos(\theta_2+\phi)} - \frac{\sin\theta_1}{\cos(\theta_1+\phi)}]} \Delta F$$

The spring tension T is then given by

$$T = \frac{\sin\theta_1}{(2/3)(13/16)^{1/2}\cos(\theta_1+\phi)}F_1 = \frac{\sin\theta_2}{(2/3)(13/16)^{1/2}\cos(\theta_2+\phi)}F_2$$

therefore the force required to activate the shuttle is

$$\text{force} = T - \frac{\sin\theta_1}{(2/3)(13/16)^{1/2}\cos(\theta_1+\phi)}F_2$$

or

$$F = T - \frac{\sin\theta_2}{(2/3)(13/16)^{1/2}\cos(\theta_1+\phi)}F_1$$

A simple computer program was written to help in the numerical solution of the above equations.

APPENDIX B

Detailed Design of the Arms

The basic analysis for the arms of the bottom mounted electric field meter was done assuming a 12 foot unsupported arm. An example, of the procedure used throughout the analysis, is included in the one piece construction analysis; a 2 inch PVC Type II pipe is considered. Figure 30 depicts the three different designs that were considered.

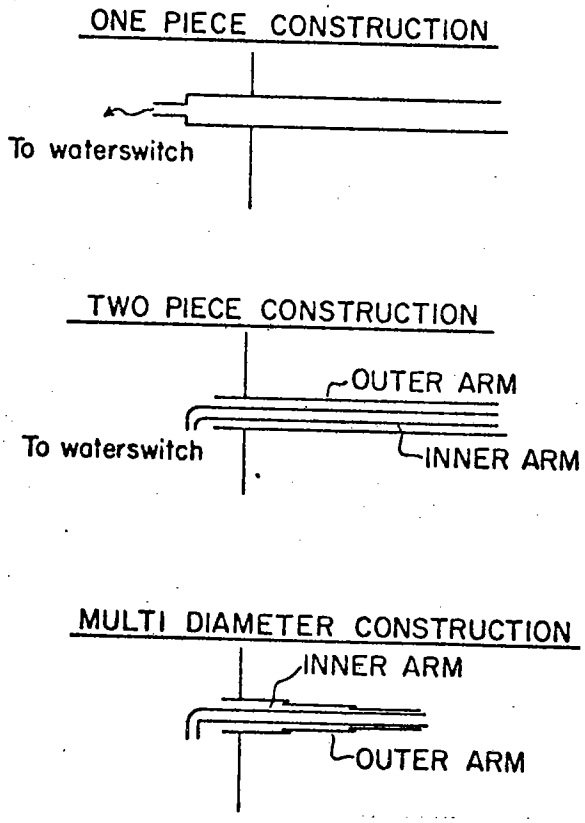

Figure 30. Types of construction used in the analysis of the arms

(A) Analysis of 12 Foot Arms - One Piece Construction - No Support

PVC Schedule 80 (Type II - High inpact)

Modulus of elasticity = 3.5 X 10^5PSI ρ75°F

Tensile strength = 6,000 PSI

Compressive strength = 8,800 PSI

Flexural strength = 11,500 PSI

The physical dimensions of the pipe to be considered are:

Pipe size = 2 in

Weight/foot = .9084 lbs.

Inside diameter = 1.939 in.

Outside diameter = 2.375 in.

Length = 12 ft.

The maximum shear in air is then the per linear foot of the pipe times its length.

Max. shear = WL

Max. shear = (.9084 lb/ft)(12 ft) = 10.9 lb

The maximum bending moment in air is then obtained by multiplying the maximum shear by one half the length of the pipe.

$$\text{Max. bending moment} = \frac{WL^2}{2}$$

Max. bending moment = (.9084 lb/ft)(12 ft)^2/2

Max. bending moment = 65.4 ft·lb

Since the radius of gyration I is given by

$$I = \pi\left(\frac{O.D.^4 - I.D.^4}{64}\right) = .868 \text{ in}^4$$

The maximum deflection in air is then

$$\text{Max. deflection} = \frac{WL^4}{8EI}$$

$$\text{Max. deflection} = \frac{(.9084\frac{lb}{ft})\ (12\ ft)^4}{(8)(3.5X10^5\frac{lb}{in^2})(.868\ in^4)}$$

$$\text{Max. deflection} = \underline{13.4\ in}$$

and the maximum stress in air is then

$$\text{Max. stress} = \frac{MC}{I}$$

$$\text{Max. stress} = \frac{(65.4\ ft\cdot lb)(2.375\ in/2)}{.868\ in^4}$$

$$\text{Max. stress} = \underline{1{,}074\ PSI}$$

A similar analysis was done for the unit stationary in sea water (the density of the sea water was assumed to be 64.15 lbs/ft^3) and for the units free fall to the bottom (the additional drag force was computed using an assumed terminal velocity of 1 meter/sec). The numerical results from these two analyses are

		Stationary In Water	Free-Fall
Max. shear	=	3 lbs	20 lbs
Max. bending moment	=	18 ft lbs	120 ft lbs
Max. deflection	=	3.7 in.	2 ft.
Max. stress	=	276 PSI	1970 PSI

Complete results for all of the pipe sizes considered are shown in Figure 31.

	Pipe Size	Shear in Air	Deflection in Air	Stationary on Bottom Shear in Sea Water	Stationary on Bottom Deflection in Sea Water	Free Fall Shear in Sea Water	Free Fall Deflection in Sea Water	1/2 Knot Current Deflection in Sea Water
	in.	lbs.	in.	lbs.	in.	lbs.	ft.	in.
Polypropylene Schedule 80	1	3.19	Fails	+.27	+5.18	Fails	Fails	20.1
	1 1/4	4.41	45.4	+.30	+3.13	Fails	Fails	11.1
Modulus of Elasticity = 1.5×10^5 PSI	1 1/2	5.34	34.0	+.37	+2.35	Fails	Fails	7.9
Tensile Strength = 4,900 PSI	2	7.34	21.2	+.51	+1.47	23.51	5.62	4.4
	2 1/2	-	-	-	-	-	-	-
Compressive Strength = 8,500 PSI	3	15.1	9.7	+1.04	+.67	34.93	1.86	1.5
Weight Per $Foot^3$ = 60.0 LBS								
PVC Schedule 80 Type II	1	4.71	47.4	1.30	13.05	Fails	Fails	8.6
	1 1/4	6.51	28.7	1.79	7.92	14.28	5.25	4.8
Modulus of Elasticity = 3.5×10^5 PSI	1 1/2	7.88	21.5	2.17	5.94	16.23	3.69	3.7
Tensile Strength = 6,000 PSI	2	10.90	13.4	3.00	3.70	20.00	2.05	1.9
	2 1/2	16.65	9.2	4.58	2.54	23.27	1.08	1.0
Compressive Strength = 8,800 PSI	3	22.27	6.1	6.13	1.68	27.76	.63	.6
Weight Per $Foot^3$ = 88.6 LBS								

Figure 31. Results of analysis - 12 foot arms, one piece construction, no support

(B) Discussion of Results - One Piece Construction - No Support

$$\text{Max. bending moment} = (.9083 \text{ lb/ft})(12 \text{ ft})^2/2$$

$$\text{Max. bending moment} = \underline{65.4 \text{ ft·lb}}$$

Since the radius of gyration I is given by

$$I = \pi\left(\frac{\text{O.D.}^4 - \text{I.D.}^4}{64}\right) = .868 \text{ in}^4$$

The maximum deflection in air is then

$$\text{Max. deflection} = \frac{WL^4}{8EI}$$

$$\text{Max. deflection} = \frac{(.9084 \frac{\text{lb}}{\text{ft}})(12 \text{ ft})^4}{(8)(3.5 \times 10^5 \frac{\text{lb}}{\text{in}^2})(.868 \text{ in}^4)}$$

$$\text{Max. deflection} = \underline{13.4 \text{ in}}$$

and the maximum stress in air is then

$$\text{Max. stress} = \frac{MC}{I}$$

$$\text{Max. stress} = \frac{(65.4 \text{ ft·lb})(2.375 \text{ in}/2)}{.868 \text{ in}^4}$$

$$\text{Max. stress} = \underline{1{,}874 \text{ PSI}}$$

It is found that the 1 in., 1 1/4 in., and 1 1/2 in. diameter, polypropylene Schedule 80, pipe would fail in shear as the instrument free-fell to the bottom at 1 meter/sec. The 2 in. diameter pipe is borderline. The only polypropylene pipe size suitable is the 3 in. diameter pipe. If the arms were constructed out of PVC the 1 in. diameter pipe would fail in shear, the 1 1/4 in. pipe is borderline, and the suitable diameters are 1 1/2 in., 2 in., 2 1/2 in. and 3 in.

(C) Analysis of 12 Foot Arms - Two Piece Construction - No Support

The outer arm in this design provides the needed strength, the inner arm provides the salt bridge. The following pipe sizes were considered in this analysis for the outer core: polypropylene 2 in. and 3 in., PVC 2 in., 2 1/2 in. and 3 in. The other pipe sizes considered previously, are not considered here because they were proven to fail. The general properties of the two inner tubings are not considered except for their weight: the specific gravity of tygon is 1.183, the specific gravity of polyethylene is .919. The inner cores are expected to be constrained in their movement by the outer shell. The results of this analysis are given in Figure 32.

(D) Discussion of Results - Two Piece Construction - No Support

It was found that 3 in. polypropylene pipe and 2 in., 2 1/2 in. and 3 in. PVC pipe with either the tygon or polyethylene inner cores are suitable. The main difference between this analysis and the previous analysis for one piece construction arms is the additional weight of the tygon and polyethylene inner cores. A close examination of the two analyses show that in air there is a 2.7 lb. increase in weight per arm if tygon is used and a 2.1 lb. increase if polyethylene is used. In water there is a .36 lb. increase in weight per arm if tygon is used and a .25 lb. decrease in weight if polyethylene is used.

(E) Analysis and Discussion of Multidiameter Arms

If a multidiameter arm is used the only combination of pipe sizes that can be used, if a 1 in. inner core is used, is 3 in., 2 in. and

Tygon Inner Core

	Pipe Site	Shear in Air	Deflection in Air	Stationary Shear in water	Stationary Reflection in water	Free Fall Shear in water	Free Fall Deflection in water
	in.	lbs.	in.	lbs.	in.	lbs.	ft.
Polyproplyene Schedule 80	2	10.1	29.0	+.2	+.43	Fails	Fails
	3	17.8	11.4	+.7	+.45	35.57	1.84
PVC Type II Schedule 80	2	13.6	16.7	3.4	4.13	19.64	2.01
	2 1/2	19.4	10.7	5.0	2.75	22.90	1.06
	3	25.0		6.5	1.78	27.40	.63

Polyethylene Inner Core

Polyproplyene Schedule 80	2	9.5	27.2	+.8	+2.18	Fails	Fails
	3	17.2	11.0	+1.3	+.83	35.18	1.87
PVC Type II Schedule 80	2	13.0	16.0	2.6	3.38	20.25	2.07
	2 1/2	18.8	10.4	4.3	2.4	23.51	1.09

Figure 32. Results of analysis - 12 foot arms, two piece construction, no support

1 1/4 in. This is the only combination that can be used because of the mismatch of outside to inside diameters of the other pipe sizes. If one takes a close look at this method of arm construction very little is achieved over the two previous methods. Also, the weight of the arm will be greater and the complexity of the arm will have increased.

(F) Analysis and Discussion of Shorter, or Supported Arms

All of the above mentioned cases were considered using a 12 foot, unsupported, length of pipe. This is indeed the worst case. It should be noted that if the arm is supported, or shortened, the maximum shear, bending moment, and stress, as well as the deflection of the arm, will vary in the following manner with the unsupported length X.

1) The maximum shear will vary in a linear fashion with X.

2) The maximum bending moment will vary as the square of X.

3) The maximum stress will vary as the square of X.

4) The maximum deflection will vary as the 4^{th} power of X.

Since the maximum stress is the major design factor, it was calculated as a function of pipe size, material, and unsupported length. The results are shown in Figure 33.

Material: Polyproplyene

unsupported length—FEET

	12	11	10	9	8
1	F	F	F	F	F
11/4	F	F	F	B	S
11/2	F	F	B	S	S
2	B	S	S	S	S
3	S	S	S	S	S

Material: Polyvynal Chloride Type II

unsupported length—FEET

	12	11	10	9	8
1	F	F	F	F	S
11/4	F	B	S	S	S
11/2	B	S	S	S	S
2	S	S	S	S	S
21/2	S	S	S	S	S
3	S	S	S	S	S

F-FAILS, B-BORDER LINE
S-SATISFACTORY

Figure 33. Results of analysis - shorter or supported arms

APPENDIX C

Electrodes

Currently there is research underway at the Woods Hole Oceanographic Institution and Lincoln Laboratory to develop field-effect transistors as a possible substitute for the silver-silver chloride electrodes presently in use in electric field meters.

The FET's in common use, and applicable to the possible substitution, are metal oxide semi-conductors (MOS) and are made of silicon. A MOS FET is constructed as indicated in Figure 34.

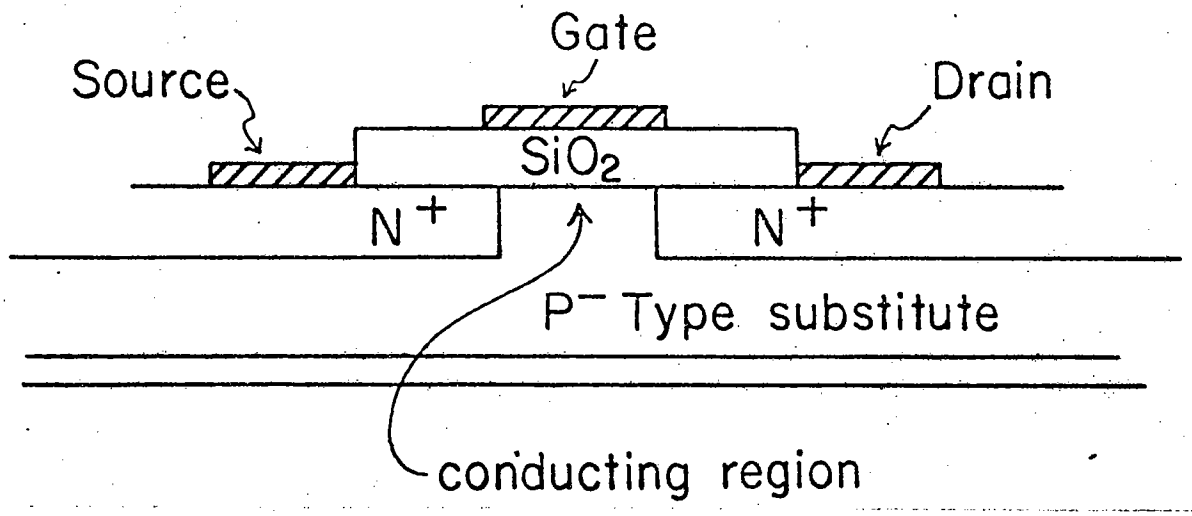

Figure 34. Field-effect transistor (MOS)

To do away with the metal electrode/sea water interface, it has been suggested by R.L. Koehler (personal communication) that the sea water make direct contact with the S_iO_2 layer. This is a field effect measurement.

FOOTNOTES

[1]Wolfgang Panofsky, and Melba Phillips, Classical Electricity and Magnetism, (Reading, Mass., Addison-Wesley Pub. Co., 1955), p. 108.

[2]M.S. Longuet-Higgins, M.E. Stern and Henry Stommel, "The Electrical Field Induced by Ocean Currents and Waves, with Applications to the Method of Towed Electrodes," Papers in Physical Oceanography and Meteorology, Vol. XIII, No. 1, (Nov., 1954), p. 12.

[3]Ibid., p. 13.

[4]William von Arx, "An Electromagnetic Method for Measuring the Velocities of Ocean Currents From a Ship Underway," Papers in Physical Oceanography and Meteorology, Vol. XI, No. 3, (Mar., 1950), p. 16.

[5]Ibid., p. 16.

[6]Thomas Sanford, "Motionally Induced Electric and Magnetic Fields in the Sea," Journal of Geophysical Research, Vol. 76, No. 15, (May 20, 1971), p. 3483.

[7]William von Arx, An Introduction to Physical Oceanography, (Reading, Mass., Addison-Wesley Pub. Co., 1962), p. 261.

[8]Robert Drever and Thomas Sanford, "A Free-Fall Electromagnetic Current Meter-Instrumentation," Proceedings of the I.E.R.E. Conference on Electronic Engineering in Ocean Technology, (London, 1970), p. 359.

[9]von Arx, An Introduction to Physical Oceanography, p. 275.

[10]Ibid. p. 275.

BIBLIOGRAPHY

1. Constant, Woodbridge, Theoretical Physics Reading, Mass., Addison-Wesley Pub. Co., 1958, pp. 171-217.

2. Drever, R.G., and Sanford, T.B., "A Free-Fall Electromagnetic Current Meter - Instrumentation," Proceedings of the I.E.R.E. Conference on Electronic Engineering in Ocean Technology," I.E.R.E., 8-9 Bedford Square, London, 1970, pp. 353-370.

3. Longuet-Higgins, M.S., "The Electrical and Magnetic Effects of Tidal Streams," Mon. Not. Roy. Astr. Soc., Geophys. Suppl., 5 (8), 1949, pp. 295-307.

4. Longuet-Higgins, M.S., Stern, M.E., and Stommel, H., "The Electric Field Induced by Ocean Currents and Waves with Applications to the Method of Towed Electrodes," Papers in Physical Oceanography and Meteorology, Vol. 13, No. 1, M.I.T. and W.H.O.I., Nov., 1954, pp. 1-37

5. Malkus, W.V.R., and Stern, M.E., "Determination of Ocean Transports and Velocities by Electromagnetic Effects," Sears Foundation: Journal of Marine Research, Vol. 11, No. 2, Nov. 15, 1952, pp. 97-105.

6. Panofsky, Wolfgang, and Phillips, Melba, Classical Electricity and Magnetism, Reading, Mass., Addison-Wesley Pub. Co., 1955, pp. 107-123.

7. Runcorn, S., "Measurements of Planetary Electric Currents," Nature, Vol. 202, 1964, pp. 10-13

8. Sanford, Thomas B., "Motionally Induced Electric and Magnetic Fields in the Sea," Journal of Geophysical Research, Vol. 76, No. 15, May 20, 1971, pp. 3476-3492.

9. Stommel, H., "Exploratory Measurements of Electric Potential Differences Between Widely Spaced Points in the North Atlantic Ocean," Archiv fur Meteorologie, Geophysik und Bioklimatologie, 7, Ser. A, 1954, pp. 292-304.

10. _____, "The Theory of the Electric Field Induced in Deep Ocean Currents," Journal of Marine Research, Vol. 7, No. 3, 1948, pp. 386-392.

11. von Arx, William S., "An Electromagnetic Method for Measuring the Velocities of Ocean Currents From a Ship Underway," Papers in Physical Oceanography and Meteorology, Vol. 11, No. 3, M.I.T. and W.H.O.I., March, 1950, pp. 1-62.

BIBLIOGRAPHY (Cont.)

12. _____, An Introduction to Physical Oceanography, Addison-Wesley Pub. Co. Reading, Mass., 1962, pp. 260-281.

13. Williams, A.J., Jaffee, R.J., Poranski, P.F., and Simonetti, P.J., Short Arm Electric Field Measurements of Ocean Currents, W.H.O.I. - 72-13, 1972, (Unpublished Manuscript).

14. Young, F.B., Gerrard, and Jevons, W., "On Electrical Disturbances Due to Tides and Waves," Phil. Mag., Ser. 6, Vol. 40, 1920, pp. 149-159.